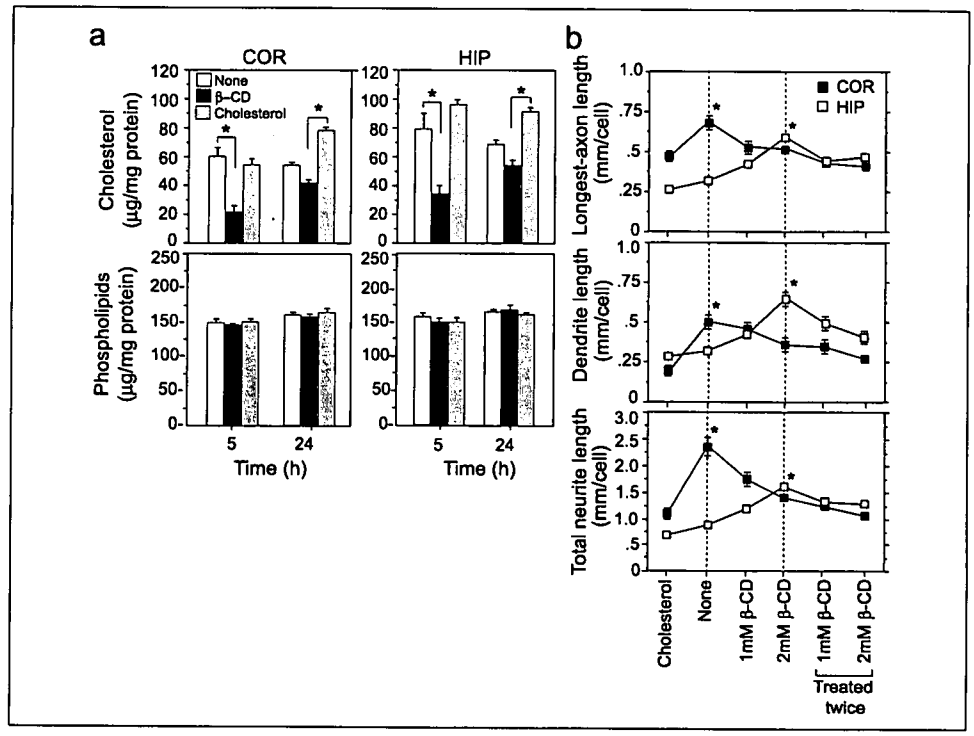

FIGURE 5. **Cholesterol concentrations in hippocampal (*HIP*) and cortical neurons (*COR*) treated with cholesterol and β-cyclodextrin.** Cultured neurons were maintained in N_2-medium for 3 days after plating, and the cultures were treated with β-CD or cholesterol as described in the legend for Fig. 3. *a*, the neurons were then harvested at 5 and 24 h following the treatment, and the concentrations of cholesterol and phospholipids in these cultures were determined as described under "Materials and Methods." The data represent mean ± S.E. Six cultures for each treatment were counted. *, $p < 0.01$. Three independent experiments showed similar results. *b*, cultured neurons maintained in N_2-medium for 3 days after plating were treated with 1 or 2 mM β-CD or 7 μg/ml cholesterol and maintained for another 2 days. Some of the cultures treated with β-CD were treated again with β-CD at the same concentration for 10 min at 37 °C and maintained for 1 additional day. All of the neurons were harvested on culture day 5 and then immunostained with the anti-tubulin antibody. Longest-axon length, total dendrite length, and neurite length per cell were determined. The data represent mean ± S.E. Twenty-five neurons were counted for each treatment. *, $p < 0.005$ *versus* 2 mM β-CD and cholesterol for cortical neurons; *, $p < 0.005$ *versus* cholesterol, no treatment (*None*), and 2 mM β-CD (twice) for hippocampal neurons. Two independent experiments showed similar results.

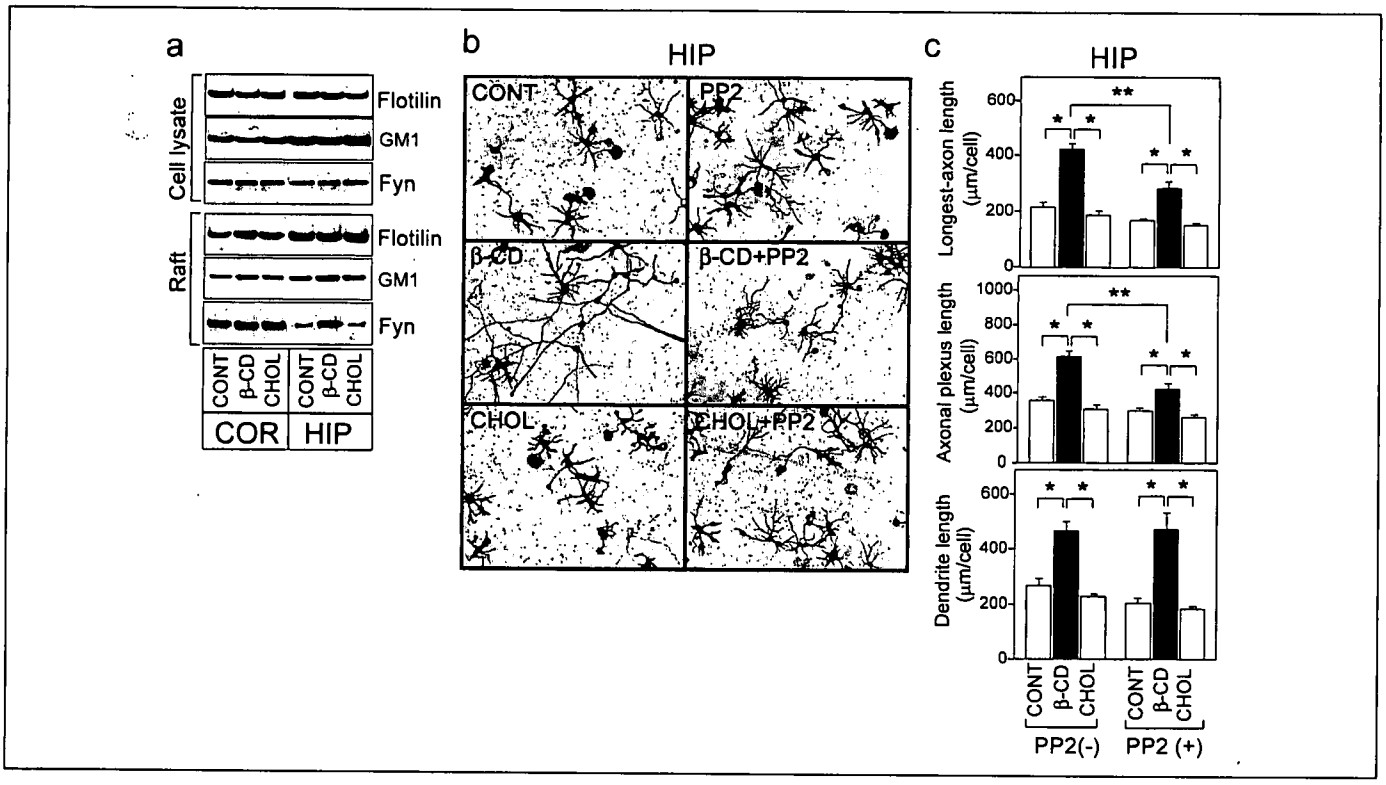

FIGURE 6. **Involvement of Fyn signaling in cholesterol-dependent modulation of axonal outgrowth in hippocampal neurons.** Cortical (*COR*) and hippocampal neurons (*HIP*) were maintained in N_2-medium for 3 days after plating, and the cultures were treated with β-CD or cholesterol (*CHOL*) as described under "Materials and Methods. *a*, the cultures were harvested after 5 days *in vitro*, and each sample was subjected to immunoblot analysis using antibodies specific for flotillin, GM1, and Fyn. *b*, hippocampal neurons were maintained in N_2-medium for 3 days after plating, and the cultures were treated with β-CD or cholesterol as described under "Materials and Methods." The hippocampal neurons were then maintained for another 2 days in the presence or absence of PP2, a Fyn signaling inhibitor, at a concentration of 5 μM. The cultures were then harvested and immunostained. *c*, longest-axon length, axonal plexus length, and dendrite length of the hippocampal neurons not treated (control (*CONT*)) or treated with β-CD or cholesterol in the presence or absence of PP2 were quantified. The data represent mean ± S.E. Twenty-five cells were analyzed for each treatment. *, $p < 0.005$; **, $p < 0.0001$. Three independent experiments showed similar results.

enhanced dendrite outgrowth induced by β-cyclodextrin was not observed (Fig. 6*c*, *bottom panel*).

DISCUSSION

This study showed that cholesterol concentration in hippocampal neurons was markedly higher than in cortical neurons and that the neurite outgrowth was significantly greater and the polarity formation occurred earlier in cortical neurons than in hippocampal neurons. In contrast, the phospholipid concentrations in these neurons were similar. Our finding that the cholesterol biosynthetic pathway is highly enhanced in hippocampal neurons compared with cortical neurons (supplemental Fig. S2) may explain the difference in cholesterol concentration between these two types of neurons.

Cholesterol depletion from hippocampal neurons markedly enhanced axon and dendrite outgrowth and accelerated the establishment of cell polarity. The morphological features appeared similar to those in cortical neurons, suggesting that a high concentration of cholesterol attenuates neurite outgrowth and polarity formation in hippocampal neurons in culture. The finding that both the loading of cholesterol to and the depletion of cholesterol from the cortical neurons attenuated neurite outgrowth suggests that there may be an optimal concentration of cholesterol for cortical neurons to exhibit neurite outgrowth (Figs. 3 and 4). This is also the case for hippocampal neurons, because the neurite outgrowth was inhibited when cholesterol was further depleted from cultured neurons by treatment with β-CD twice (Fig. 5*b*).

The cholesterol concentration in the Triton X-100-insoluble fraction from hippocampal neurons was greater than that from cortical neurons, whereas cholesterol concentration in the Triton X-100-soluble fraction did not differ between these two types of neurons, indicating that the difference in the concentration of cholesterol in the Triton X-100-insoluble fraction may explain the neuron-specific difference in total cholesterol concentration between these two types of neurons. This notion is supported by the finding that cholesterol concentration in lipid rafts isolated from hippocampal neurons is higher than in those from cortical neurons (Fig. 2). In contrast to cholesterol concentration, phospholipid concentration did not show any difference between these two types of neurons. This also suggests that neuronal differentiation and neurite outgrowth in hippocampal neurons may be modulated by cholesterol in lipid rafts and raft-localized molecules and that the morphological difference between cortical and hippocampal neurons can be explained by the difference in cholesterol concentration between these neurons.

The mechanism by which a decreased level of cholesterol in lipid rafts modulates neurite outgrowth has not been completely understood. However, the finding that the enhancement of neurite outgrowth induced by β-cyclodextrin treatment is accompanied by the recruitment of Fyn to lipid rafts and that the Src family inhibitor PP2 inhibits axonal elongation induced by β-cyclodextrin treatment suggests that an increased level of raft-localized Fyn is in part involved in β-cyclodextrin-induced axonal elongation in hippocampal neurons. This notion is supported by previous studies showing that Src family kinases, including Fyn, play a critical role in axon outgrowth (27, 28) and that lipid raft-localized Fyn is more catabolically active than non-raft-localized Fyn (29, 30).

Another interesting point is that cellular cholesterol concentration modulates the development of hippocampal neurons but not that of cortical neurons (Fig. 3), although it modulates neurite outgrowth in both types of neurons (Figs. 4 and 5). As demonstrated previously (26), neurons initially establish several apparently identical, short processes. With culture time, one of the processes begins to grow very rapidly and becomes an axon, and the other processes then become dendrites. Interestingly, the establishment of neuronal polarity in hippocampal neurons depends on cellular cholesterol concentration; a decreased cholesterol concentration stimulates the establishment of neuronal polarity, whereas an increased concentration of cellular cholesterol inhibits it. This is not the case for cortical neurons. The present study does not provide any explanation for the discrepancy in the cell type-specific regulation of polarity formation mediated by cholesterol. This may suggest that cholesterol is not the only lipid responsible for the observed alterations and that membrane composition is relevant for cortical neurons. Further study is required to clarify the mechanism underlying the cell type-specific regulation of polarity formation mediated by cholesterol.

Recent studies have shown that cholesterol supplied as an apoE-lipoprotein complex to neurons via apoE receptors plays a critical role in synaptogenesis, neurite outgrowth, and neuronal repair (9–11). Most of the published literature is concerned with only a single neuronal subtype, which is not sufficient for the appreciation of the complex role of cholesterol in neurons. The present study shows that cholesterol demand and the optimal cholesterol concentration for neurite outgrowth depend completely on the neuronal type and that the mechanism underlying the effect of cholesterol on neuronal maturation involves the attainment of the optimal cholesterol concentration. There are issues that need to be elucidated to delineate the mechanisms underlying the neuronal type-specific regulation of neurite outgrowth by cellular cholesterol concentration, and it is required to confirm that the present findings are also the case *in vivo*. However, the present study suggests that the role of cholesterol in relation to neuronal phenotypes and functions should be elucidated in a neuron type- and brain region-specific manner.

REFERENCES

1. Schwarz, A., Rapaport, E., Hirschberg, K., and Futerman, A. H. (1995) *J. Biol. Chem.* **270**, 10990–10998
2. Ledesma, M. D., Simons, K., and Dotti, C. G. (1998) *Proc. Natl. Acad. Sci. U. S. A.* **95**, 3966–3971
3. Ledesma, M. D., Brugger, B., Bunning, C., Wieland, F. T., and Dotti, C. G. (1999) *EMBO J.* **18**, 1761–1771
4. Simons, K., and Toomre, D. (2000) *Nat. Rev. Mol. Cell Biol.* **1**, 31–39
5. Fan, Q.-W., Yu, W., Gong, J. S., Zou, K., Sawamura, N., Senda, T., Yanagisawa, K., and Michikawa, M. (2002) *J. Neurochem.* **80**, 178–190
6. Fan, Q. W., Yu, W., Senda, T., Yanagisawa, K., and Michikawa, M. (2001) *J. Neurochem.* **76**, 391–400
7. Goodrum, J. F., Brown, J. C., Fowler, K. A., and Bouldin, T. W. (2000) *J. Neuropathol. Exp. Neurol.* **59**, 1002–1010
8. Karten, B., Vance, D. E., Campenot, R. B., and Vance, J. E. (2003) *J. Biol. Chem.* **278**, 4168–4175
9. Hayashi, H., Campenot, R. B., Vance, D. E., and Vance, J. E. (2004) *J. Biol. Chem.* **279**, 14009–14015
10. Mauch, D. H., Nagler, K., Schumacher, S., Goritz, C., Muller, E. C., Otto, A., and Pfrieger, F. W. (2001) *Science* **294**, 1354–1357
11. Koudinov, A. R., and Koudinova, N. V. (2001) *FASEB J.* **15**, 1858–1860
12. Braak, H., and Braak, E. (1997) *Neurobiol. Aging* **18**, 351–357
13. Price, J. L., and Morris, J. C. (1999) *Ann. Neurol.* **45**, 358–368
14. Katsuno, T., Morishima-Kawashima, M., Saito, Y., Yamanouchi, H., Ishiura, S., Murayama, S., and Ihara, Y. (2005) *Neurology* **64**, 687–692
15. Simons, M., Keller, P., Dichgans, J., and Schulz, J. B. (2001) *Neurology* **57**, 1089–1093
16. Simons, M., Keller, P., De Strooper, B., Beyreuther, K., Dotti, C. G., and Simons, K. (1998) *Proc. Natl. Acad. Sci. U. S. A.* **95**, 6460–6464
17. Fassbender, K., Simons, M., Bergmann, C., Stroick, M., Lutjohann, D., Keller, P., Runz, H., Kuhl, S., Bertsch, T., von Bergmann, K., Hennerici, M., Beyreuther, K., and Hartmann, T. (2001) *Proc. Natl. Acad. Sci. U. S. A.* **98**, 5856–5861
18. Sawamura, N., Gong, J. S., Garver, W. S., Heidenreich, R. A., Ninomiya, H., Ohno, K., Yanagisawa, K., and Michikawa, M. (2001) *J. Biol. Chem.* **276**, 10314–10319
19. Bu, B., Li, J., Davies, P., and Vincent, I. (2002) *J. Neurosci.* **22**, 6515–6525
20. Suzuki, K., Parker, C. C., Pentchev, P. G., Katz, D., Ghetti, B., D'Agostino, A. N., and

Carstea, E. D. (1995) *Acta Neuropathol. (Berl.)* **89**, 227–238
21. Michikawa, M., and Yanagisawa, K. (1999) *J. Neurochem.* **72**, 2278–2285
22. Yu, W., Gong, J. S., Ko, M., Garver, W. S., Yanagisawa, K., and Michikawa, M. (2005) *J. Biol. Chem.* **280**, 11731–11739
23. Gong, J. S., Kobayashi, M., Hayashi, H., Zou, K., Sawamura, N., Fujita, S. C., Yanagisawa, K., and Michikawa, M. (2002) *J. Biol. Chem.* **277**, 29919–29926
24. Lisanti, M. P., Scherer, P. E., Vidugiriene, J., Tang, Z., Hermanowski-Vosatka, A., Tu, Y. H., Cook, R. F., and Sargiacomo, M. (1994) *J. Cell Biol.* **126**, 111–126
25. Sawamura, N., Ko, M., Yu, W., Zou, K., Hanada, K., Suzuki, T., Gong, J. S., Yanagisawa, K., and Michikawa, M. (2004) *J. Biol. Chem.* **279**, 11984–11991
26. Dotti, C. G., Sullivan, C. A., and Banker, G. A. (1988) *J. Neurosci.* **8**, 1454–1468
27. Meriane, M., Tcherkezian, J., Webber, C. A., Danek, E. I., Triki, I., McFarlane, S., Bloch-Gallego, E., and Lamarche-Vane, N. (2004) *J. Cell Biol.* **167**, 687–698
28. Liu, G., Beggs, H., Jurgensen, C., Park, H. T., Tang, H., Gorski, J., Jones, K. R., Reichardt, L. F., Wu, J., and Rao, Y. (2004) *Nat. Neurosci.* **7**, 1222–1232
29. Mukherjee, A., Arnaud, L., and Cooper, J. A. (2003) *J. Biol. Chem.* **278**, 40806–40814
30. Shima, T., Nada, S., and Okada, M. (2003) *Proc. Natl. Acad. Sci. U. S. A.* **100**, 14897–14902

THE JOURNAL OF BIOLOGICAL CHEMISTRY
© 2005 by The American Society for Biochemistry and Molecular Biology, Inc.
Vol. 280, No. 29, Issue of July 22, pp. 27296–27302, 2005
Printed in U.S.A.

Neurodegeneration in Heterozygous Niemann-Pick Type C1 (NPC1) Mouse

IMPLICATION OF HETEROZYGOUS NPC1 MUTATIONS BEING A RISK FOR TAUOPATHY*

Received for publication, April 11, 2005, and in revised form, May 18, 2005
Published, JBC Papers in Press, May 25, 2005, DOI 10.1074/jbc.M503922200

Wenxin Yu, Mihee Ko, Katsuhiko Yanagisawa, and Makoto Michikawa‡

From the Department of Alzheimer's Disease Research, National Institute for Longevity Sciences, 36-3 Gengo, Morioka, Obu, Aichi 474-8522, Japan

Niemann-Pick type C1 (NPC1) disease is an autosomal recessive, fatal disorder characterized by a defect in cholesterol trafficking and progressive neurodegeneration. The disease is predominantly caused by mutations in the *NPC1* gene; however, it has been assumed that heterozygous *NPC1* mutations do not cause any symptoms. Here we demonstrate that cholesterol accumulation does not occur in young mouse brains; however, it does in aged (104–106-week-old) NPC1+/− mouse brains. In addition, Purkinje cell loss was observed in aged NPC1+/− mouse cerebellums. Immunoblot analysis using anti-phospho-tau antibodies (AT-8, AT-100, AT-180, AT-270, PHF-1, and SMI-31) demonstrates the site-specific phosphorylation of tau at Ser-199, Ser-202, Ser-212, and Thr-214 in the brains of aged NPC1+/− mice. Mitogen-activated protein kinase, a potential serine kinase known to phosphorylate tau, was activated, whereas other serine kinases, including glycogen synthase kinase 3β, cyclin-dependent kinase 5, or stress-activated protein kinase/c-Jun N-terminal kinase were not activated. Cholesterol level in the lipid raft isolated from the cerebral cortices, ATP level, and ATP synthase activity in the cerebral cortices significantly decreased in the aged NPC1+/− brains compared with those in the NPC1+/+ brains. All of these changes observed in NPC1+/− brains were determined to be associated with aging and were not observed in the age-matched NPC1+/+ brains. These results clearly demonstrate that heterozygous NPC1 impairs neuronal functions and causes neurodegeneration in aged mouse brains, suggesting that human heterozygous NPC1 mutations may be a risk factor for neurodegenerative disorders, such as tauopathy, in the aged population.

Niemann-Pick type C1 (NPC1)[1] disease is an autosomal recessive disorder characterized by progressive neurodegeneration including ataxia, dystonia, seizures, and dementia (1). In NPC1-deficient cells, exogenously transported and endogenously synthesized cholesterol accumulate in late endosome/lysosomes, with delayed cholesterol transport to cellular compartments responsible for the regulation of intracellular cholesterol homeostasis (2–5). In addition to cholesterol, glycosphingolipids and other lipids accumulate in homozygous NPC1 brains with aging (1, 6). The gene responsible for NPC1 disease, *NPC1*, was cloned in both humans and mice (7, 8). It was previously demonstrated that NPC1 plays a key role in the transport of cholesterol to the *trans*-Golgi network, plasma membrane, and endoplasmic reticulum (9–12).

The neuropathological features of NPC1 brains are characterized by the loss of neurons such as Purkinje cells, hyperphosphorylated tau, and neurofibrillary tangle formation with the accumulation of lipid storage bodies and the presence of dendritic and axonal abnormalities (6, 13–16). These lines of evidence suggest that the intracellular accumulation of cholesterol and gangliosides correlates with the progression of NPC1 disease and induces neurodegeneration. However, there is a different viewpoint on the pathogenesis of NPC1 disease; *i.e.* the continuous defective use of cholesterol in NPC1 neural tissues causes tauopathy (6, 16, 17). This notion is supported by previous studies showing that there is cholesterol deficiency in cellular compartments including distal axons (18), although cholesterol accumulation occurs in the late endosome/lysosomal compartment (4, 5) due to a defect in the transport of cholesterol, the source of which is either endogenous synthesis or exogenous uptake.

With respect to neuronal gangliosides, a previous study supports the notion that the accumulation of gangliosides causes neurodegeneration (19), whereas another study indicates that the accumulation of gangliosides is not the cause of neurodegeneration in NPC1 mice (20). A recent study has demonstrated that impaired neurosteroidogenesis, due to disordered cholesterol trafficking, affects neuronal growth and differentiation and that allopregnanolone treatment delays the onset of neurological symptoms and lengthens the life of NPC1 mice (21).

Our recent study has shown a novel mechanism underlying neurodegeneration in NPC1 disease, whereby an increased cholesterol level in mitochondrial membranes adversely affects mitochondrial membrane potential, the synthesis of ATP, and the level of cellular ATP in NPC1 mouse brains and neurons (22). Since mitochondria are a key organelle for steroidogenesis, mitochondrial dysfunction may responsible for impaired neurosteroidogenesis. In addition, this also indicates that not whole-cell cholesterol level but rather compartment- or organelle-associated cholesterol level is critical for maintaining neuronal functions.

* This work was supported by grants from the Ministry of Health, Labor, and Welfare of Japan (Comprehensive Research on Aging and Health Grant H14-10 and Research on Human Genome and Tissue Engineering Grant H17-004), by the Pharmaceuticals and Medical Devices Agency, Japan, and by the National Niemann-Pick Disease Foundation, USA. The costs of publication of this article were defrayed in part by the payment of page charges. This article must therefore be hereby marked "*advertisement*" in accordance with 18 U.S.C. Section 1734 solely to indicate this fact.

‡ To whom correspondence should be addressed. Tel.: 81-562-46-2311; Fax: 81-562-46-3157; E-mail: michi@nils.go.jp.

[1] The abbreviations used are: NPC1, Niemann-Pick type C1; MAPK, mitogen-activated protein kinase; ERK, extracellular signal-regulated kinase; GSK-3β, glycogen synthase kinase 3β; SAPK, stress-activated protein kinase; JNK, c-Jun N-terminal kinases; Cdk5, cyclin-dependent kinase 5; PBS, phosphate-buffered saline; GM1, Galβ1-3Gal-NAcβ1-4Gal(3-2αNeuAc)β1-4Glcβ1-1Cer.

This paper is available on line at http://www.jbc.org

Note that NPC1 disease is an autosomal recessive disease, and heterozygous carriers of NPC1 mutations are not assumed to develop any neurological symptoms during their entire life span, and note that the effect of heterozygous NPC1 mutations on the development of neurological disorders has not been extensively investigated. This is also the case for NPC1+/− mice. However, intermediate abnormalities in terms of cholesterol metabolism have been shown in nonneuronal cells from NPC1 patients (23–25) and in nonneuronal tissues or cells from NPC1+/− mice (26–28). In addition, our recent study has demonstrated that NPC1+/− exhibits intermediate dysfunction in the mitochondria of the brains of NPC1+/− mice at 9 weeks of age (22). These lines of evidence have led us to examine whether there occurs neuronal dysfunction or damage in NPC1+/− mouse brains under certain conditions such as aging.

In this study, morphological and biochemical studies were performed on brains of aged heterozygous NPC1+/− mice. In contrast to what has been assumed, neurodegeneration as demonstrated by Purkinje cell loss, enhanced phosphorylation of tau, and activated MAPK/ERK1/2 were clearly observed in NPC1+/− mouse brains. It has been assumed that mutant NPC1 heterozygotes do not develop any clinical symptoms; however, these results suggest that heterozygous NPC1 mutations may be a risk factor for tauopathy. Since it is estimated that the incidence of NPC1 disease is as high as 1:150,000 (1), the percentage of the total population with the heterozygous NPC1 mutation is estimated to be around 0.5%. Thus, our present results show that heterozygous NPC1 mutations unexpectedly affect brains with aging and thus may lead to the investigation of the link between heterozygous NPC1 mutations and neurodegenerative diseases, such as Alzheimer disease.

EXPERIMENTAL PROCEDURES

BALB/c NPC1NIH Mice—The animal care and experiments using animals performed in this study were carried out in accordance with institutional guidelines. BALB/c mice carrying the genetic mutation for NPC1 were obtained from The Jackson Laboratory (Bar Harbor, ME). These heterozygous mice were bred to acquire NPC1+/+ and NPC1+/− mice used in this study. The genotypes of the mice were determined from genomic DNA isolated from tail snip DNA using a PCR-based method and oligonucleotide primers described previously (7). PCR products were separated using a 1.2% agarose gel. The mice used in this study ranged from 104 to 106 weeks of age.

Reagents—The monoclonal anti-phospho-independent tau antibody T46 was obtained from Zymed Laboratories, Inc. (South San Francisco, CA). The monoclonal anti-tau antibodies AT8 (specific for phospho-Ser^{199} and -Ser^{202}), AT-100 (specific for phospho-Ser^{212} and -Thr^{214}), AT180 (specific for phospho-Thr^{231}), and AT-270 (specific for phospho-Thr^{181}) were purchased from Innogenetics (Ghent, Belgium). The monoclonal anti-tau antibody SMI31 (specific for phospho-Ser^{396}) was purchased from Sternberger Monoclonals Inc. (Baltimore, MD). The monoclonal anti-tau antibody, PHF-1 (specific for phospho-Ser^{396} and -Ser^{404}), was kindly provided by Dr. P. Davies (Albert Einstein College of Medicine). Rabbit polyclonal antibodies specific for phospho-MAPK/ERK1/2 (specific for phospho-Thr^{202} and -Tyr^{204}), pan-MAPK/ERK1/2, phospho-SAPK/JNK, and pan-SAPK/JNK and a monoclonal antibody recognizing phospho-GSK-3β (specific for phospho-Tyr^{279} and -Tyr^{216}) were purchased from Cell Signaling Technology (Beverly, MA). The monoclonal anti-phospho-independent GSK-3β antibody was purchased from BD Transduction Laboratories (Lexington, KY). The rabbit anti-p35 antibody, which reacts with the p35 and p25 regulatory subunits of cyclin-dependent kinase 5 (Cdk5), was obtained from Santa Cruz Biotechnology, Inc. (Santa Cruz, CA). The polyclonal anti-calbindin D28K was obtained from Chemicon International (Temecula, CA). The monoclonal anti-flotillin-1 antibody and anti-β-tubulin antibody were purchased from Covance (Richmond, CA) and BD Transduction Laboratories (San Jose, CA), respectively. Horseradish peroxidase-conjugated cholera toxin B and the filipin complex were purchased from Sigma.

Histological Analysis—The mice were sacrificed by CO_2 inhalation and perfused intracardially with 0.1 M phosphate-buffered saline (PBS) containing heparin (50 units/ml). The brains were removed and fixed in 4% paraformaldehyde in PBS overnight at 4 °C and then rinsed with PBS and cryoprotected in a solution of 30% sucrose in PBS. Fixed tissues were sectioned on a semimotorized rotary microtome (LEICA RM2145, Wetzlar, Germany) at 30 μm and processed for immunohistochemistry with the anti-calbindin D28K (1:500) and AT8 (1:500). Immunoreactivity was detected with diaminobenzidine using the ABC Elite kit according to the manufacturer's instructions (Vector Laboratories, Burlingame, CA). For cresyl violet staining, slides were immersed in 70, 80, and 95%, ethanol for 5 min each and in 100% ethanol for 5 min and then in xylene for 15 min. The slides were then sequentially immersed back in 100, 95, and 70% ethanol solutions and distilled water for 5 min in each. The slides were stained for 1 min in filtered cresyl violet solution and then briefly rinsed twice in distilled water. They were then sequentially dehydrated again in 70, 80, 95, and 100% ethanol solutions for 2 min each. The slides were placed in xylene for another 10 min and then mounted with Permount. For double fluorescence staining, the sections were treated overnight with calbindin D28K antibody (1:500) and AT-8 antibody (1:500) at 4 °C overnight, followed by incubation with second antibodies, rhodamine-conjugated goat anti-rabbit IgG (Chemicon International, Temecura, CA) diluted at 1:500, and fluorescein isothiocyanate-conjugated goat anti-mouse IgG (American Qualex, San Clemente, CA) diluted at 1:50, for 1 h at room temperature. The slides were then washed with PBS and mounted with Vectashield (Vector). For costaining with calbindin D28K antibody and filipin, the sections were incubated overnight with calbindin D28K antibody (1:500) at 4 °C overnight, followed by washing three times for 5 min each using 100 μg/ml filipin in PBS and then incubated with rhodamine-conjugated goat anti-rabbit IgG (1:500) for 1 h at room temperature. The slides were then washed with PBS and mounted with Vectashield (Vector). Fluorescent images were obtained using a model LSM 510 laser-scanning confocal microscope (Zeiss) equipped with a × 63 Plan Apochromat numerical aperture and a 1.4 oil immersion objective.

Protein Preparation—The mice were sacrificed by CO_2 inhalation, and their brains were harvested, rinsed in PBS, and immediately frozen in liquid nitrogen. The cerebrum and cerebellum were separated and homogenized in 10 volumes of Tris-saline (50 mM Tris-HCl (pH 7.4) and 150 mM NaCl), containing protease inhibitors (Complete™) and phosphatase inhibitors (10 μM NaF and 1 mM orthovanadate) using a motor-driven Teflon homogenizer. The homogenates were centrifuged at 3,000 × *g* for 10 min at 4 °C, and the supernatants were stored for biochemical analyses. Protein concentration was determined using the bicinchoninic acid protein assay kit (Pierce).

Determination of ATP Level—ATP level in mouse brain tissues was determined as previously reported (22). In brief, the homogenates of cerebrum and cerebellum were centrifuged at 10,000 rpm for 2 min at 4 °C and then rinsed three times with PBS. ATP level in these samples was determined using the ATP Bioluminescence Assay kit CLS II (Roche Applied Science). In brief, the pellet was resuspended in 50 μl of ice-cold ATP lysis buffer (100 mM Tris and 4 mM EDTA, pH 7.75), to which 150 μl of boiling ATP lysis buffer was added, and the samples were incubated for 2 min at 99 °C. The samples were centrifuged at 10,000 rpm for 1 min at 4 °C, and the supernatants were collected. Finally, the ATP level was determined by combining 50 μl of the supernatant with 50 μl of the luciferase reagent. After a 20-s delay, chemiluminescence was measured with a 2.6-s integration time using a microplate luminometer (EG&G Berthold, Bad Wildbad, Germany). Luciferase activity was expressed in fluorescence units/μg of protein.

Determination of ATP Synthase Activity—Brain mitochondria were isolated as previously reported (22). For the determination of ATP synthase activity, 100 μg of mitochondrial protein from each sample was used to measure the rate of ATP synthesized. The reaction was initiated by adding 100 μg of mitochondrial protein into 100 μl of reaction buffer (10 mM K_2HPO_4 (pH 7.4) 300 mM D-mannitol, 10 mM KCl, and 5 mM $MgCl_2$) at 37 °C. After 1 min, 10 μl of ADP (50 μM) was added, and the intensity of bioluminescence was recorded at 37 °C, where peak height was proportional to the amount of ATP synthesized.

Immunoblot Analysis—Equal amounts of proteins separated using 4–20% gradient Tris/Tricine SDS–PAGE (Dai-ichi Pure Chemical Co., Ltd., Tokyo, Japan) were electrophoretically transferred onto a polyvinylidene difluoride membrane (Millipore Corp., Bedford, MA). Nonspecific binding was blocked with 5% fat-free milk in phosphate-buffered saline containing 0.1% Tween 20. The blots were then incubated with primary antibodies overnight at 4 °C. For the detection of both monoclonal and polyclonal antibodies, appropriate peroxidase-conjugated secondary antibodies were used in conjunction with SuperSignal chemiluminescence (Pierce) to obtain images on the film.

Preparation of Raft Fractions—Detergent-insoluble membrane raft fractions were obtained according to the established method previously

reported (6). One milliliter of each fraction was sequentially collected from the top of the gradient. The extraction of lipids and the subsequent determination of the amounts of cholesterol and phospholipids in each sample were carried out according to previously described methods (29).

Lipid Analysis—The levels of cholesterol and phospholipids in the samples were determined using enzymatic methods. Cholesterol level was determined using a cholesterol determination kit, LTCII (Kyowa Medex, Tokyo), whereas phospholipid level was determined using a phospholipid determination kit, PLB (Wako, Osaka, Japan).

Detection of GM1 Ganglioside—For the detection of GM1 ganglioside, samples from each fraction were dissolved in equal volumes of Laemmli buffer. They were then subjected to 4–20% gradient Tris/Tricine SDS-PAGE (Dai-ichi Pure Chemical Co., Ltd.). The separated GM1 ganglioside was transferred onto an Immobilon or polyvinylidene difluoride membrane (Millipore) with a semidry electrophoretic transfer apparatus (Nihon Eido, Tokyo, Japan) using a transfer buffer (0.1 M Tris, 0.192 M glycine, and 20% methanol). The membranes were blocked with 5% fat-free milk in PBS containing 0.1% Tween 20 for 1 h and probed with horseradish peroxidase-conjugated cholera toxin B (Sigma) (final concentration of 42 ng/ml) overnight at 4 °C. In between steps, the membranes were washed four times with PBS-T for 15 min. Bound cholera toxin was detected using Super Signal Chemiluminescence (Pierce).

Statistical Analysis—Statistical analysis was carried out using StatView computer software (Macintosh version 5.0, Abacus Concepts Inc., Berkeley, CA). A p value of <0.05 was considered to be significant.

RESULTS

Cholesterol Accumulation in Brains of Aged NPC1 Heterozygous Mouse—The brains of NPC1+/+ and NPC1+/− mice at 24, 40, and 104–106 weeks of age were isolated, and the levels of cholesterol and phospholipids were determined. The cholesterol levels in the cerebrum and cerebellum of the NPC1+/− mice were significantly elevated compared with those in the same brain areas of the NPC1+/+ mice at 104–106 weeks of age (Fig. 1*a*), whereas the cholesterol levels were similar in the two groups at 24 and 40 weeks of age (Fig. 1*a*). The phospholipid levels were similar in the two genotypes at every age examined (Fig. 1*b*). The filipin and calbindin staining of brain samples (the third lobe of each cerebellum) prepared from the NPC1+/+ and NPC1+/− mice at 104 weeks of age shows that cells exhibiting a strong filipin-positive signal in the NPC1+/− cerebellar section (from the third lobe) are also calbindin-positive, whereas the calbindin-positive cells in the NPC1+/+ cerebellar section exhibit a very weak signal for filipin staining (Fig. 1*c*). These results indicate that cholesterol accumulation occurs in Purkinje cells of aged NPC1+/− mouse cerebellum.

Purkinje Cell Loss in Aged NPC1 Heterozygous Mice—The cerebellums of NPC1+/+ and NPC1+/− mice at 104–106 weeks of age were immunohistochemically analyzed using the anti-calbindin antibody, which specifically recognizes Purkinje cells. The number of anti-calbindin antibody-positive cells decreased in the NPC1+/− cerebrum (Fig. 2, *d–f*) compared with that in the NPC1+/+ cerebellum (Fig. 2, *a–c*), suggesting that Purkinje cell loss occurred in the aged NPC1+/− cerebellum. However, this was not the case for the NPC1+/− cerebellum at 24 and 40 weeks of age (data not shown). Next, the number of anti-calbindin antibody-positive cells in each lobe of the cerebellums of the NPC1+/+ and NPC1+/− mice at 104–106 weeks of age was determined. The number of Purkinje cells was significantly decreased in first + second, third, seventh, and eighth lobes of NPC1+/− cerebellum compared with those of NPC1+/+ cerebellum (Fig. 2*g*).

Hyperphosphorylation of Tau in NPC1+/− Mouse Brain—Since neurodegeneration found in the NPC homozygous mouse brain is accompanied by hyperphosphorylated tau (6, 16), the sagittal sections of the brains were immunohistochemically stained using the anti-phospho-tau antibody AT-8. AT-8 stained neurons strongly in the cerebral cortices and hippocampus of the NPC1+/− mice (Fig. 3, *b* and *d*) compared with those of the NPC1+/+ mice (Fig. 3, *a* and *c*). For cerebellar sections,

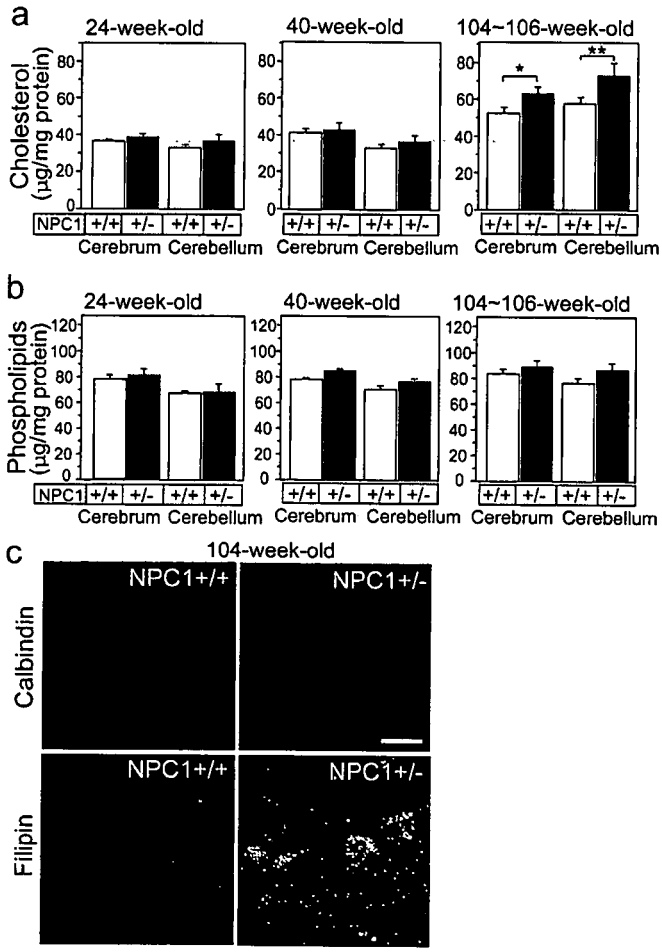

FIG. 1. **Cholesterol accumulation in aged NPC1+/− mouse brains.** Cholesterol and phospholipids were extracted from the brains of the NPC1+/+ and NPC1+/− mice at 24, 40, and 104–106 weeks of age, and their levels were determined. The levels of cholesterol (*a*) and phospholipids (*b*) per mg of protein are shown. *, $p < 0.04$; **, $p < 0.01$. The results represent the mean ± S.E. of three different samples and are representative of three independent experiments. *c*, brain sections from the third lobes of each cerebellum of NPC1+/+ and NPC1+/− mice at 104 weeks old were subjected to filipin and calbindin staining as described under "Experimental Procedures" and visualized using confocal laser microscopy. Purkinje neurons demonstrated as calbindin-positive cells in NPC1+/− mouse cerebellum were strongly stained with filipin, whereas those in NPC1+/+ mouse cerebellum were only weakly stained. *Scale bar*, 25 μm.

double staining using anti-calbindin antibody was performed. The Purkinje cells demonstrated as being calbindin-positive were very faintly stained with AT-8 in the aged NPC1+/− mouse cerebellum, whereas calbindin-positive Purkinje cells were also AT-8-positive in the aged NPC1+/+ mouse cerebellum (Fig. 3, *e–h*). The ratio of AT-8-positive Purkinje cells to total Purkinje cells was very high in NPC1+/− mouse cerebella compared with that of NPC1+/+ mouse cerebella (Fig. 3*i*).

To verify that the histologic abnormalities are a result of enhanced tau phosphorylation, immunoblot analysis was conducted using lysates of the NPC1+/+ and NPC1+/− cerebrums and cerebellums. The antibodies used were T-46, which recognizes phospho-independent tau; AT-8, AT-100, AT-180, AT-270, PHF-1, and SMI-31, which recognize site-specific phosphorylation of tau; and the anti-β-tubulin antibody as an internal standard. The intensities of the signals corresponding to phosphorylated tau demonstrated by AT-8 and AT-100 increased in the cerebrum and cerebellum of the NPC1+/− mice at 104–106 weeks of age compared with those for the NPC1+/+ mice of at the same age (Fig. 4*a*). However, the intensities of the signals

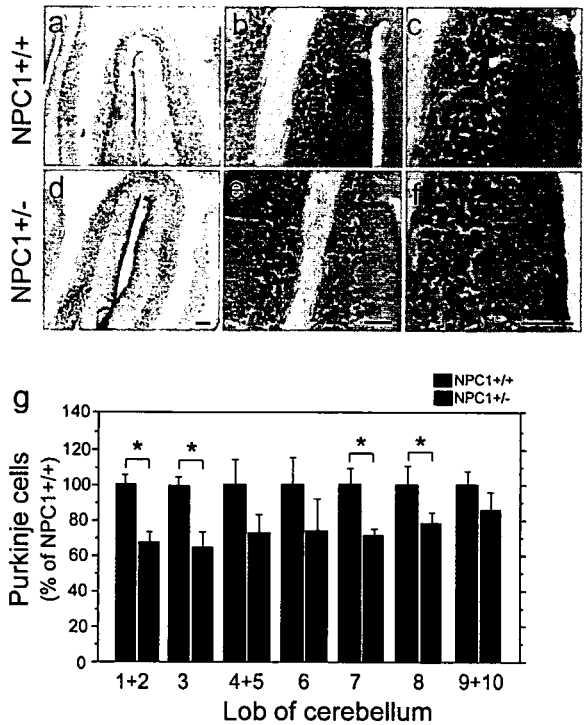

FIG. 2. **Cerebellar histology in aged NPC1+/− mouse brains.** Brain sections (cerebellum) from the NPC1+/+ and NPC1+/− mice at 104–106 weeks old were subjected to immunohistochemistry using the anti-calbindin antibody D28, as described under "Experimental Procedures." Calbindin-immunoreactive neurons in the third lobes of the cerebellum of NPC1+/+ (*a–c*) and NPC1+/− (*d–f*) are shown on different scales. *Scale bars*, 100 μm. *g*, the number of calbindin-immunopositive neurons was determined in all of the cerebellar lobes of the NPC1+/+ and NPC1+/− mice. 20 sections prepared from the NPC1+/+ and NPC1+/− mice were counted. Each section contained 489 ± 45 Purkinje cells for the NPC1+/+ cerebellum and 346 ± 24 Purkinje cells for the NPC1+/− cerebellum. Data are presented as a percentage of the number of Purkinje neurons in the NPC1+/+ mice (n = 5 for each genotype). *, $p < 0.05$.

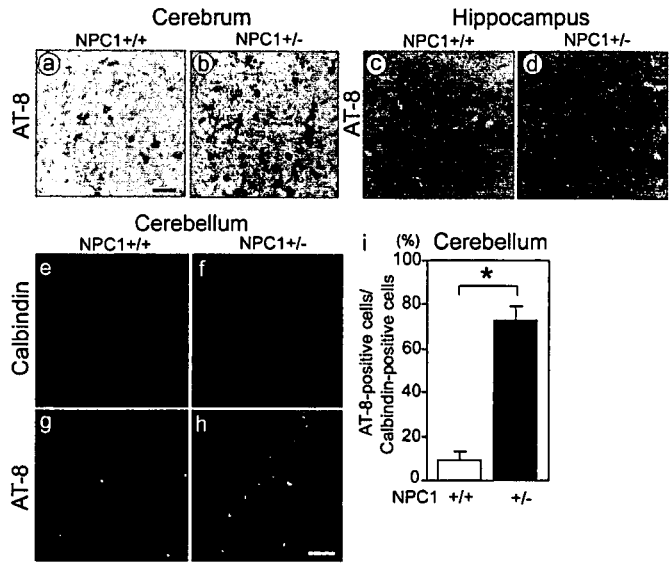

FIG. 3. **Immunohistochemical analysis of cerebral, hippocampal, and cerebellar sections of 104–106-week-old NPC1+/+ and NPC1+/− mice.** *a–d*, cerebral and hippocampal sections were subjected to immunohistochemical analysis using the phospho-tau antibody AT-8, as described under "Experimental Procedures," and visualized with diaminobenzidine using the ABC Elite kit. *e–h*, for cerebellar sections, double staining using AT-8 and anti-calbindin antibody was performed. AT-8-positive neurons were visualized with fluorescein isothiocyanate-conjugated second antibody, and calbindin-positive neurons were visualized with rhodamine-conjugated second antibody. *i*, the numbers of AT-8-positive cells in 50 calbindin-positive cells were counted, and the ratio of AT-8-positive cells to calbindin-positive cells was calculated. Data represent the mean ± S.E. of six samples. *, $p < 0.001$. *Scale bar*, 50 μm.

demonstrated by AT-180, AT-270, PHF-1, and SMI-31 did not differ between samples from the NPC1+/+ and NPC1+/− brains (Fig. 4*a*). The phosphorylation site of tau in the cerebrums and cerebellums of the NPC1+/+ and NPC1+/− mice at 24 and 40 weeks of age was also determined (Fig. 4, *b* and *c*, respectively). The phosphorylation state of tau and the total tau level in both samples demonstrated by AT-8 and T-46 did not differ between the NPC1+/+ and NPC1+/− mice (Fig. 4, *b* and *c*).

MAPK Was Activated in NPC1+/− Mouse Brains—Since our previous reports demonstrated that tau phosphorylation in NPC1-deficient cells is caused by enhanced MAPK activity (6, 17), the activity of tau kinases including MAPK was determined. Among the kinases examined, including MAPK/ERK1/2, GSK-3β, JNK, and Cdk5/p25, the levels of phospho-MAPK/ERK1/2 in the cerebrum and cerebellum of the NPC1+/− mice at 104–106 weeks of age increased compared with those for the NPC1+/+ mice (Fig. 5*a*), whereas the levels of phospho-GSK-3β, -JNK, and Cdk5/p25 remained unchanged (Fig. 5, *b*, *c*, and *d*). The activities of MAPK/ERK1/2 in the cerebrums and cerebellums of the NPC1+/+ and NPC1+/− mice at 24 and 40 weeks of age were also determined. The activities of MAPK/ERK1/2 in both samples did not differ between the NPC1+/+ and NPC1+/− mice (Fig. 5, *e* and *f*).

Cholesterol Level in Lipid Rafts Decreased in NPC1+/− Mouse Brains—Because the enhanced MAPK/ERK1/2 activity due to the decreased cholesterol level in the lipid rafts is suggested to induce tau phosphorylation in NPC1−/− mouse brains and NPC1−/− cells (6, 17), lipid compositions in the raft fractions isolated from the cerebral cortices of the NPC1+/+ and NPC1+/− mice were analyzed. The raft marker GM1 ganglioside was recovered in fractions 4 and 5, and another raft marker, flotillin-1, was recovered in fraction 5 (Fig. 6*c*). The cholesterol levels in fractions 4 and 5 isolated from the NPC1+/− brain were significantly lower than those in the same fractions isolated from the NPC1+/+ brain (Fig. 6*a*), whereas the levels of phospholipids in these fractions showed no significant difference between the two genotypes (Fig. 6*b*).

Level of ATP in NPC1+/+ and NPC1+/− Brains—Our previous study demonstrated that ATP levels in NPC1−/− organs including the brain, liver, and muscles as well as in NPC1−/− cultured neurons decrease compared with those in NPC1+/+ organs and neurons (22); thus, ATP level and ATP synthase activity in the aged NPC1+/+ and NPC1+/− brains were determined. As shown in Fig. 7, ATP levels in the cerebrum and cerebellum of the NPC1+/− mice at 104–106 weeks of age significantly decreased compared with those in the same brain areas of the NPC1+/+ mice (Fig. 7*a*). ATP synthase activity in the cerebellum of the aged NPC1+/− mice also decreased compared with that of the aged NPC1+/+ mice (Fig. 7*b*).

DISCUSSION

Here we demonstrate for the first time the unexpected phenomenon that neurodegeneration occurs in aged NPC1+/− mouse brains. This neuronal damage is accompanied by tau hyperphosphorylation and enhanced MAPK/ERK1/2 activity, which are observed in young NPC1−/− mouse brains and NPC1−/− cells (6, 17). The significant accumulation of cholesterol in neurons in the brain and the significant reduction in cholesterol level in raft fractions isolated from aged NPC1+/− cerebrums were also observed. These changes are found to depend on aging in NPC1+/− mice.

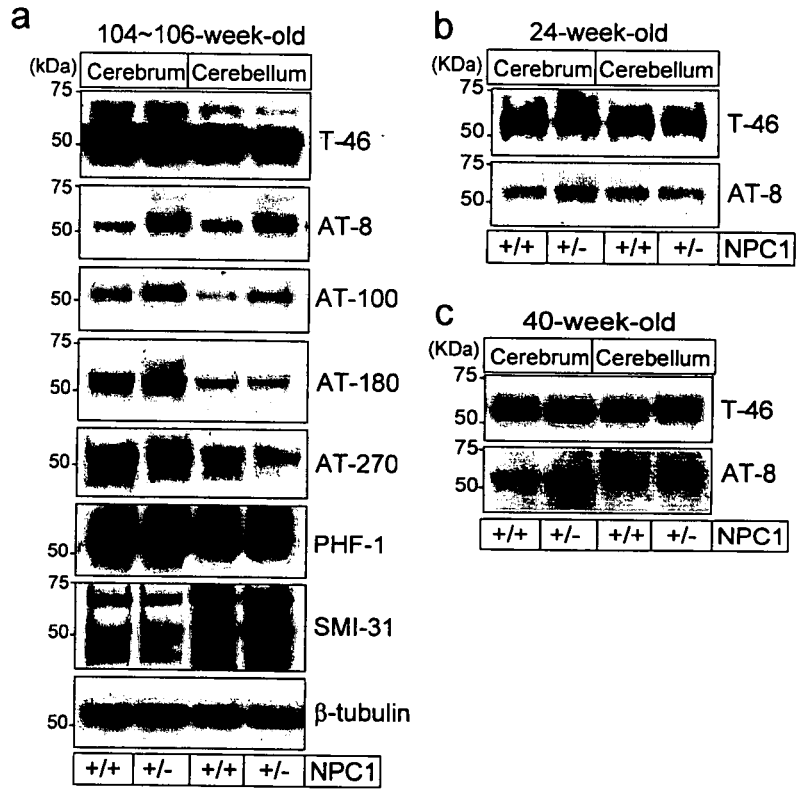

FIG. 4. **Immunoblot analysis of tau in cerebrum and cerebellum of 104–106-week-old NPC1+/+ and NPC1+/− mice.** *a*, equal amounts of postnuclear supernatant protein from the cerebrum and cerebellum were subjected to immunoblot analysis using the site-specific phospho-tau antibodies AT-8, AT-100, AT-180, AT-270, PHF-1, and SMI-31 in addition to an antibody that recognizes phospho-independent tau, T46, and the anti-β-tubulin antibody as an internal standard. Tau in the cerebrum and cerebellum of 24-week-old (*b*) and 40-week-old (*c*) NPC1+/+ and NPC1+/− mice was immunohistochemically analyzed using AT-8 and AT-100 antibodies.

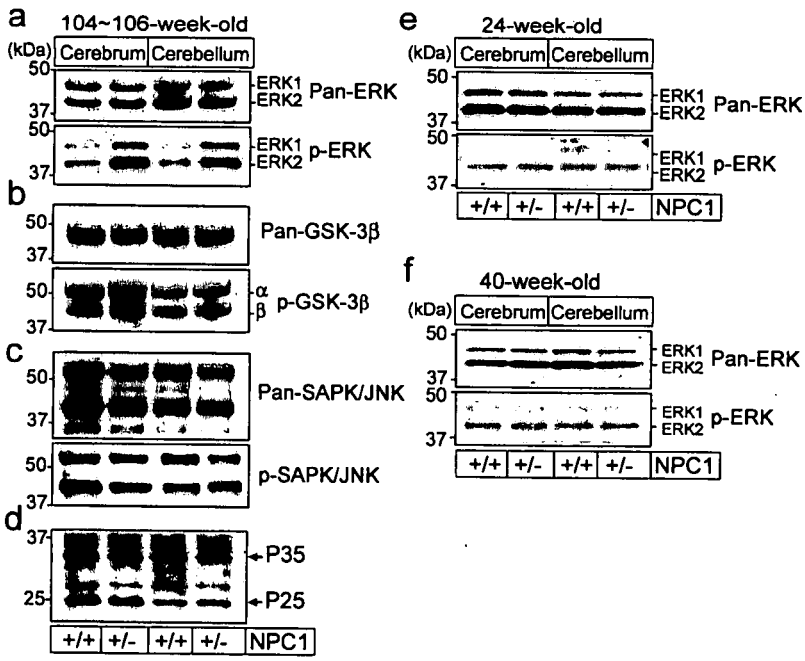

FIG. 5. **Immunoblot analysis of tau-directed kinases in cerebrum and cerebellum of 104–106-week-old NPC1+/+ and NPC1+/− mice.** Equal amounts of postnuclear supernatant protein from the cerebrum and cerebellum were subjected to immunoblot analysis using the monoclonal antibodies specific for pan-ERK1/2 and phospho-ERK (*p-ERK*) (*a*), pan-GSK-3β and phospho-GSK-3β (*p-GSK-3β*) (*b*), pan-SAPK/JNK and phospho-SAPK/JNK (*p-SAPK/JNK*) (*c*), and Cdk5 (*d*). Immunoblot analysis of ERK1/2 in the cerebrum and cerebellum of 24-week-old (*e*) and 40-week-old (*f*) NPC1+/+ and NPC1+/− mice was performed using anti-pan-ERK and anti-phospho-ERK antibodies.

NPC1 disease is a hereditary disorder that develops in an autosomal recessive manner; thus, it has been assumed that heterozygous carriers of NPC1 mutations do not develop any neurological symptoms during their entire life span (1). It has also been presumed that this is the case for NPC1+/− model mice. Therefore, little attention has been paid to whether NPC1+/− mice develop any symptoms with aging. To our surprise, however, the present study has clearly shown that neurodegeneration demonstrated as Purkinje cell loss accompanied by intracellular cholesterol accumulation and its deficiency in lipid rafts occurs in the aged NPC1+/− mouse brain. A few studies have investigated NPC1 heterozygotes and have shown that NPC1 heterozygotes have "intermediate" abnormalities in cholesterol metabolism at the nonneuronal cell level (23, 26, 27); however, it has been shown that there is no significant abnormality in terms of cholesterol metabolism in cultured NPC1+/− neurons (30) and young NPC1+/− brains (6). These lines of evidence suggest that cholesterol metabolism in the central nervous system changes and neurodegeneration accompanied by abnormal tau phosphorylation occurs only in aged NPC1+/− mice. The reason for the change in cholesterol metabolism found only in the aged NPC1+/− brains may be the expression of the NPC1 protein in NPC1+/− brains being approximately half that in NPC1+/+ brains (6), which may

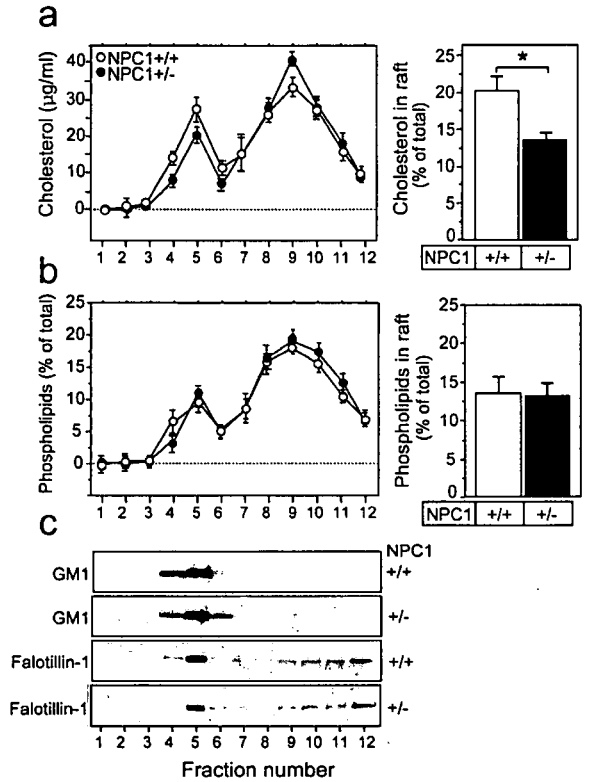

FIG. 6. **Distribution of cholesterol and phospholipids in raft fractions from brains of 104–106-week-old NPC1+/+ and NPC1+/− mice.** The cell homogenates of the cerebellar cortices of 104–106-week-old NPC1+/+ and NPC1+/− mice in the presence of 1% Triton X-100 were subjected to sucrose density gradient ultracentrifugation. The levels of cholesterol (*a*) and phospholipids (*b*) in each fraction were determined, and the distribution of such components across the fractions is shown. *c*, distribution of GM1 ganglioside and flotillin-1, markers for lipid rafts, across the fractions was determined as described under "Experimental Procedures." The levels of cholesterol (*a*, *right panel*) and phospholipids (*b*, *right panel*) in fractions 4 and 5 (raft fractions) are shown. Data represent the mean ± S.E. of six samples. Two independent experiments showed similar results. *, $p < 0.04$

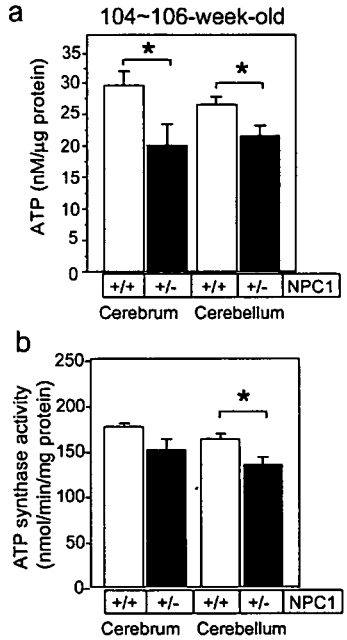

FIG. 7. **ATP level and ATP synthase activity in brains of 104–106-week-old NPC1+/+ and NPC1+/− mice.** *a*, ATP level was determined in the cerebrum and cerebellum isolated from the NPC1+/+ and NPC1+/− mice at 104–106 weeks of age. For each of the samples, equal amounts of protein were used to compare ATP level. Data show mean ± S.E. of five samples. Two independent experiments show similar results. *b*, the ATP synthase activities in mitochondria isolated from cerebrum and cerebellum of the NPC1+/+ and NPC1+/− mice at 104–106 weeks of age was determined. The fraction containing purified brain mitochondria was isolated as described previously (22). The enzymatic analysis was performed by measuring the rate of ATP synthesis from ADP (ATP synthesis). The results represent the mean ± S.E. of five different samples and are representative of two independent experiments. *, $p < 0.05$.

very slightly affect cellular cholesterol trafficking. As a result, it takes a longer time for neurons to show any abnormalities in terms of cholesterol accumulation in the late endosome/lysosome compartment and the subsequent shortage of cholesterol in other compartments.

Since a decreased cellular cholesterol level stimulates MAPK activity (17, 31) and tau phosphorylation (32), it is reasonable to postulate that a reduced cholesterol level in lipid rafts, due to impaired cholesterol trafficking, increases MAPK activity and enhances tau phosphorylation in aged NPC1+/− brains. This is the case for younger NPC1−/− brains; *i.e.* neurodegeneration in NPC1−/− brains is linked with an increased MAPK activity and enhanced tau phosphorylation induced by a sustained cholesterol shortage due to the absence of its trafficking (6, 17).

In addition, it is likely that impaired cholesterol trafficking and the resultant intracellular cholesterol accumulation may result in an increased cholesterol level in mitochondria, which induces mitochondrial dysfunction, thereby affecting ATP synthase activity and reducing cellular ATP level, because, as we have reported, both increased and decreased cholesterol level in the mitochondrial membrane cause mitochondrial dysfunction and reduce cellular ATP level, which causes neurodegeneration in the younger NPC1−/− mice (22). With these results taken together, it is possible that the altered cellular cholesterol metabolism enhances tau phosphorylation and decreases cellular ATP level, both of which synergistically or independently induce neuronal neurodegeneration. One may raise the questions of what causes neurodegeneration, enhanced tau phosphorylation or low ATP level, and whether these two pathways work independently or dependently. The present study cannot answer these questions. Previous studies demonstrated that mitochondrial dysfunction with energy depletion causes cell death (33, 34) and that tau abnormalities alone can cause neurodegenerative diseases (35, 36), indicating that each pathway can independently cause neuronal death. However, previous studies showed that there is a correlation between ATP level and the activity of tau kinases including MAPK/ERK1/2 (37, 38). These results enable us to assume that mitochondrial dysfunction with a decreased ATP level and the enhancement of tau phosphorylation synergistically contribute to neurodegeneration in aged NPC1+/− mouse brains.

Finally, the results of our present study, contrary to what has been assumed, suggest that heterozygous NPC1 mutations are a risk for neuronal impairment. Since the ratio of the population with heterozygous NPC1 mutations is estimated to be as high as 0.5% (1), our findings lead us to further examine whether heterozygous NPC1 mutations are a risk for tauopathy, including Alzheimer disease. These issues should be addressed in future studies.

REFERENCES

1. Patterson, M. C., Vanier, M. T., Suzuki, K., Morris, J. A., Carstea, E. D., Neufeld, E. B., Blanchette Mackie, E. J., and Pentchev, P. G. (2001) in *The Metabolic and Molecular Basis of Inherited Disease* (Scriver, C. R., Beaudet, A. L., Sly, W. S., and Valle, D., eds) pp. 3611–3633, McGraw-Hill Inc., New York
2. Liscum, L., Ruggiero, R. M., and Faust, J. R. (1989) *J. Cell Biol.* **108**, 1625–1636
3. Pentchev, P. G., Kruth, H. S., Comly, M. E., Butler, J. D., Vanier, M. T., Wenger, D. A., and Patel, S. (1986) *J. Biol. Chem.* **261**, 16775–16780

4. Kobayashi, T., Beuchat, M. H., Lindsay, M., Frias, S., Palmiter, R. D., Sakuraba, H., Parton, R. G., and Gruenberg, J. (1999) *Nat. Cell Biol.* **1,** 113–118
5. Cruz, J. C., and Chang, T. Y. (2000) *J. Biol. Chem.* **275,** 41309–41316
6. Sawamura, N., Gong, J. S., Garver, W. S., Heidenreich, R. A., Ninomiya, H., Ohno, K., Yanagisawa, K., and Michikawa, M. (2001) *J. Biol. Chem.* **276,** 10314–10319
7. Loftus, S. K., Morris, J. A., Carstea, E. D., Gu, J. Z., Cummings, C., Brown, A., Ellison, J., Ohno, K., Rosenfeld, M. A., Tagle, D. A., Pentchev, P. G., and Pavan, W. J. (1997) *Science* **277,** 232–235
8. Carstea, E. D., Morris, J. A., Coleman, K. G., Loftus, S. K., Zhang, D., Cummings, C., Gu, J., Rosenfeld, M. A., Pavan, W. J., Krizman, D. B., Nagle, J., Polymeropoulos, M. H., Sturley, S. L., Ioannou, Y. A., Higgins, M. E., Comly, M., Cooney, A., Brown, A., Kaneski, C. R., Blanchette-Mackie, E. J., Dwyer, N. K., Neufeld, E. B., Chang, T. Y., Liscum, L., Strauss, J. F., III, Ohno, K., Zeigler, M., Carmi, R., Sokol, J., Markie, D., O'Neill, R. R., van Diggelen, O. P., Elleder, M., Patterson, m. C., Brady, R. O., Vanier, M. T., Pentchev, P. G., and Tagle, D. A. (1997) *Science* **277,** 228–231
9. Liscum, L., and Klansek, J. J. (1998) *Curr. Opin. Lipidol.* **9,** 131–135
10. Neufeld, E. B., Wastney, M., Patel, S., Suresh, S., Cooney, A. M., Dwyer, N. K., Roff, C. F., Ohno, K., Morris, J. A., Carstea, E. D., Incardona, J. P., Strauss, J. F., III, Vanier, M. T., Patterson, M. C., Brady, R. O., Pentchev, P. G., and Blanchette-Mackie, E. J. (1999) *J. Biol. Chem.* **274,** 9627–9635
11. Garver, W. S., Heidenreich, R. A., Erickson, R. P., Thomas, M. A., and Wilson, J. M. (2000) *J. Lipid Res.* **41,** 673–687
12. Wojtanik, K. M., and Liscum, L. (2003) *J. Biol. Chem.* **278,** 14850–14856
13. Suzuki, K., Parker, C. C., Pentchev, P. G., Katz, D., Ghetti, B., D'Agostino, A. N., and Carstea, E. D. (1995) *Acta Neuropathol.* **89,** 227–238
14. Love, S., Bridges, L. R., and Case, C. P. (1995) *Brain* **118,** 119–129
15. Auer, I. A., Schmidt, M. L., Lee, V. M., Curry, B., Suzuki, K., Shin, R. W., Pentchev, P. G., Carstea, E. D., and Trojanowski, J. Q. (1995) *Acta Neuropathol.* **90,** 547–551
16. Bu, B., Li, J., Davies, P., and Vincent, I. (2002) *J. Neurosci.* **22,** 6515–6525
17. Sawamura, N., Gong, J. S., Chang, T. Y., Yanagisawa, K., and Michikawa, M. (2003) *J. Neurochem.* **84,** 1086–1096
18. Karten, B., Vance, D. E., Campenot, R. B., and Vance, J. E. (2003) *J. Biol. Chem.* **278,** 4168–4175
19. Walkley, S. U., Siegel, D. A., Dobrenis, K., and Zervas, M. (1998) *Ann. N. Y. Acad. Sci.* **845,** 188–199
20. Liu, Y., Wu, Y. P., Wada, R., Neufeld, E. B., Mullin, K. A., Howard, A. C., Pentchev, P. G., Vanier, M. T., Suzuki, K., and Proia, R. L. (2000) *Hum. Mol. Genet.* **9,** 1087–1092
21. Griffin, L. D., Gong, W., Verot, L., and Mellon, S. H. (2004) *Nat. Med.* **10,** 704–711
22. Yu, W., Gong, J. S., Ko, M., Garver, W. S., Yanagisawa, K., and Michikawa, M. (2005) *J. Biol. Chem.*
23. Kruth, H. S., Comly, M. E., Butler, J. D., Vanier, M. T., Fink, J. K., Wenger, D. A., Patel, S., and Pentchev, P. G. (1986) *J. Biol. Chem.* **261,** 16769–16774
24. Vanier, M. T., Wenger, D. A., Comly, M. E., Rousson, R., Brady, R. O., and Pentchev, P. G. (1988) *Clin. Genet.* **33,** 331–348
25. Vanier, M. T., Rodriguez-Lafrasse, C., Rousson, R., Gazzah, N., Juge, M. C., Pentchev, P. G., Revol, A., and Louisot, P. (1991) *Biochim. Biophys. Acta* **1096,** 328–337
26. Garver, W. S., Krishnan, K., Gallagos, J. R., Michikawa, M., Francis, G. A., and Heidenreich, R. A. (2002) *J. Lipid Res.* **43,** 579–589
27. Choi, H. Y., Karten, B., Chan, T., Vance, J. E., Greer, W. L., Heidenreich, R. A., Garver, W. S., and Francis, G. A. (2003) *J. Biol. Chem.* **278,** 32569–32577
28. Feng, B., Zhang, D., Kuriakose, G., Devlin, C. M., Kockx, M., and Tabas, I. (2003) *Proc. Natl. Acad. Sci. U. S. A.* **100,** 10423–10428
29. Michikawa, M., Fan, Q. W., Isobe, I., and Yanagisawa, K. (2000) *J. Neurochem.* **74,** 1008–1016
30. Henderson, L. P., Lin, L., Prasad, A., Paul, C. A., Chang, T. Y., and Maue, R. A. (2000) *J. Biol. Chem.* **275,** 20179–20187
31. Wang, P. Y., Liu, P., Weng, J., Sontag, E., and Anderson, R. G. (2003) *EMBO J.* **22,** 2658–2667
32. Fan, Q. W., Yu, W., Senda, T., Yanagisawa, K., and Michikawa, M. (2001) *J. Neurochem.* **76,** 391–400
33. Green, D. R., and Reed, J. C. (1998) *Science* **281,** 1309–1312
34. Lang-Rollin, I. C., Rideout, H. J., Noticewala, M., and Stefanis, L. (2003) *J. Neurosci.* **23,** 11015–11025
35. Hutton, M., Lendon, C. L., Rizzu, P., Baker, M., Froelich, S., Houlden, H., Pickering-Brown, S., Chakraverty, S., Isaacs, A., Grover, A., Hackett, J., Adamson, J., Lincoln, S., Dickson, D., Davies, P., Petersen, R. C., Stevens, M., de Graaff, E., Wauters, E., van Baren, J., Hillebrand, M., Joosse, M., Kwon, J. M., Nowotny, P., Che, L. K., Norton, J., Morris, J. C., Reed, L. A., Trojanowski, J., Basun, H., Lannfelt, L., Neystat, M., Fahn, S., Dark, F., Tannenberg, T., Dodd, P. R., Hayward, N., Kwok, J. B., Schofield, P. R., Andreadis, A., Snowden, J., Craufurd, D., Neary, D., Owen, F., Oostra, B. A., Hardy, J., Goate, A., van Swieten, J., Mann, D., Lynch, T., and Heutink, P. (1998) *Nature* **393,** 702–705
36. Poorkaj, P., Bird, T. D., Wijsman, E., Nemens, E., Garruto, R. M., Anderson, L., Andreadis, A., Wiederholt, W. C., Raskind, M., and Schellenberg, G. D. (1998) *Ann. Neurol.* **43,** 815–825
37. Bush, M. L., Miyashiro, J. S., and Ingram, V. M. (1995) *Proc. Natl. Acad. Sci. U. S. A.* **92,** 1861–1865
38. Mizukami, Y., Iwamatsu, A., Aki, T., Kimura, M., Nakamura, K., Nao, T., Okusa, T., Matsuzaki, M., Yoshida, K., and Kobayashi, S. (2004) *J. Biol. Chem.* **279,** 50120–50131

Journal of Neuroscience Research 80:114–119 (2005)

Oligomerization of Amyloid β-Protein Occurs During the Isolation of Lipid Rafts

Wenxin Yu,[1] Kun Zou,[1] Jian-Sheng Gong,[1,2] Mihee Ko,[1] Katsuhiko Yanagisawa,[1] and Makoto Michikawa[1]*

[1]Department of Alzheimer's Disease Research, National Institute for Longevity Sciences, Aichi, Japan
[2]The Organization of Pharmaceutical Safety and Research of Japan, Tokyo, Japan

Cholesterol- and glycosphingolipid-rich microdomains, called "lipid rafts," are suggested to initiate and promote the pathophysiology of Alzheimer's disease by serving as a platform for generation, aggregation, or degradation of amyloid-β protein (Aβ). However, methods for biochemical isolation of these microdomains may produce artifacts. In this study, when synthetic Aβ1–40 monomers were added to the brain fragment at a final concentration of 2.1 μM, followed by homogenization and isolation of lipid rafts by an established method, Aβ1–40 accumulated as oligomers in the lipid raft fraction. However, in the absence of a brain homogenate, synthetic Aβ1–40 did not accumulate in the lipid raft fraction. When fractionation was performed in the absence of synthetic Aβ1–40 and synthetic Aβ1–40 was incubated in an aliquot of each fraction, a marked oligomerization of Aβ1–40 was observed in the lipid raft aliquot. These results indicate that exogenous Aβ associates with lipid rafts, and Aβ bound to rafts forms oligomers during the isolation of lipid rafts. In addition, endogenous Aβ1–40 in a Triton X-100-insoluble fraction of a brain homogenate of the Tg2576 transgenic mouse model of Alzheimer's disease formed oligomers when the fraction was incubated at 4°C for 20 hr. Thus, one should be careful when one discusses the role of lipid rafts in amyloid precursor protein processing and in the generation, aggregation, and degradation of Aβ.
© 2005 Wiley-Liss, Inc.

Key words: lipid rafts; Aβ; oligomers; cholesterol; sphingolipids; Alzheimer's disease

Alzheimer's disease (AD) is a slowly progressive neurodegenerative disease accompanied by dementia and psychological symptoms (Alzneimer, 1907). Extracellular deposits of the amyloid-β protein (Aβ) consisting of 39–43-amino-acid peptides, the intracellular formation of neurofibrillary tangles composed of highly phosphorylated tau, and synaptic dysfunction accompanied by neurodegeneration are the major pathological findings in AD brains (Alzneimer, 1907). The mechanism underlying the initiation of the pathological process of AD is postulated to be the age-related aggregation of Aβ (Selkoe, 1994; Esiri et al., 1997). This amyloid hypothesis, that is, aggregated/fibrous Aβ initiates and promotes AD pathophysiologies that lead to the development of AD symptoms, has dominated for years in the AD research field, and extensive effort has focused on how the generation and aggregation of Aβ are modulated and on the roles of Aβ in the pathogenesis of AD. Several lines of evidence partially support this notion by showing that highly aggregated Aβ fibrils, but not Aβ monomers, induce AD pathologies in vitro and in vivo (Mattson et al., 1993; Pike et al., 1993; Lorenzo and Yankner, 1994; Estus et al., 1997; Geula et al., 1998; Gotz et al., 2001; Morishima et al., 2001). However, recent lines of evidence have shown that not highly aggregated Aβ but, rather, smaller assemblies or oligomers of Aβ have the ability to disrupt neuronal functions, leading to neurodegeneration (Lambert et al., 1998; Hartley et al., 1999; Michikawa et al., 2001; Walsh et al., 2002; Sponne et al., 2003).

It has been shown that the cellular concentrations of cholesterol and sphingolipid modulate amyloid precursor protein (APP) processing and Aβ generation (Simons et al., 1998; Kojro et al., 2001; Sawamura et al., 2004) as well as the state of tau phosphorylation, synaptic plasticity, and neurodegeneration (Fan et al., 2001; Koudinov and Koudinova, 2001; Sawamura et al., 2001). These findings highlighted the role of lipid rafts, which are microdomains of the plasma membrane and contain high concentrations of cholesterol and sphingolipids (Simons and Ikonen, 1997). Lipid rafts exist as liquid-ordered regions of the membrane that are resistant to extraction with nonionic detergents and play important roles in signal transduction, cell adhesion, and lipid/protein sorting (Sargiacomo et al., 1993; Simons and Ikonen, 1997; Bagnat et al., 2000). Recent lines of evidence have shown that lipid rafts play a critical role in APP processing and in the generation and aggregation/deposition of Aβ (Lee et al., 1998; Morishima-Kawashima and Ihara, 1998; Oshima et al., 2001; Ehehalt et al., 2003; Kawarabayashi et al., 2004). However, it has also been suggested that meth-

Contract grant sponsor: Ministry of Health, Labor and Welfare of Japan; Contract grant number: Longevity Sciences Grant H14-10; Contract grant sponsor: Pharmaceuticals and Medical Devices Agency, Japan.

*Correspondence to: Makoto Michikawa, MD, Department of Alzheimer's Disease Research, National Institute for Longevity Sciences, 36-3 Gengo, Morioka, Obu, Aichi 474-8522, Japan. E-mail: michi@nils.go.jp

Received 21 September 2004; Revised 8 November 2004; Accepted 30 December 2004

Published online 9 February 2005 in Wiley InterScience (www.interscience.wiley.com). DOI: 10.1002/jnr.20428

© 2005 Wiley-Liss, Inc.

ods for the biochemical isolation of these microdomains produce artifacts (Harder and Simons, 1997), which limits our interpretation of results obtained by a biochemical method of isolating lipid rafts.

Here we experimentally determined whether isolation of lipid rafts affects the accumulation and aggregation of Aβ in the lipid raft fraction by using synthetic Aβ1–40. We found that the biochemical isolation of lipid rafts promotes Aβ oligomerization. These results suggest that one should be careful when interpreting the results of APP processing and Aβ metabolism in lipid rafts isolated by a classical biochemical method.

MATERIALS AND METHODS

Immunoblot Analysis

For the detection of Aβ, proteins separated by using 4–20% gradient Tris/tricine SDS-PAGE were electrophoretically transferred onto a nitrocellulose membrane. Highly sensitive immunoblotting was performed as described previously (Sudoh et al., 1998). For the detection of flotilin-1, a raft marker, and transferrin receptor, a nonraft marker, proteins separated using SDS-PAGE were electrophoretically transferred onto a polyvinylidene difluoride membrane (Millipore, Bedford, MA). Nonspecific binding was blocked with 5% fat-free milk in phosphate-buffered saline containing 0.1% Tween 20 (PBS-T). The blots were then incubated with a primary antibody overnight at 4°C. The monoclonal antibodies used were BA27, which is specific for the Aβ1–40 C-terminal site (Asami-Odaka et al., 1995), antiflotilin-1 antibody (BD Transduction Lab, San Jose, CA), and antitransferrin receptor antibody (Zymed, San Francisco, CA). The membrane was then incubated with a goat anti-mouse peroxidase-conjugated secondary antibody and visualized with SuperSignal chemiluminescence (Pierce, Rockford, IL) to obtain images on a film. For the detection of GM1 ganglioside, the membrane was probed with horseradish peroxidase-conjugated cholea toxin B (Sigma, St. Louis, MO; final concentration of 42 ng/ml) overnight at 4°C.

Isolation of Lipid Rafts From Rat Brain Cortex With or Without Synthetic Aβ1–40

An SD rat was anesthetized and its brain removed. One hundred milligrams of the isolated cerebral cortex were used for lipid raft isolation. The cerebral cortex in a glass/Teflon homogenizer tube (Iuchi, Osaka, Japan) was homogenized in 2.2 ml 1% Triton X-100/MBS [25 mM 2-(*N*-Morpholino) ethanesulfonic acid (MES) and 150 mM NaCl (pH 6.5) with 1% Triton X-100], including a mixture of protease inhibitors (Complete; Boehringer Mannheim, Mannheim, Germany), with or without 2.1 μM synthetic human Aβ1–40 (Peptide Institute Inc., Osaka, Japan). The brain fragments were homogenized with a glass/Teflon homogenizer (Iuchi) with 10 up-and-down strokes at 3,000 rpm on ice. The homogenates were then sonicated at 4°C and incubated for 1 hr on ice. The final Aβ1–40 concentration in the homogenate mixture was 2.1 μM. To prepare a stock solution of Aβ1–40, 0.5 mg Aβ1–40 was dissolved in 60 μl dimethylsulfoxide (DMSO), and the solution was then diluted with PBS to a final concentration of 200 μM. The lipid raft fraction was obtained from each homogenate as reported previously (Lisanti et al., 1994; Sawamura et al., 2001). One milliliter of each fraction was sequentially collected from the top of the gradient. The extraction of lipids and the subsequent determination of the concentration of cholesterol and phospholipids in each sample were carried out as reported previously (Michikawa et al., 2001).

Isolation of the Triton X-100-Insoluble Fraction From Tg2576 Mouse Brain

The Tg2576 mouse model of AD (Hsiao et al., 1996) at 13 months of age was anesthetized and the brain was removed. One hundred milligrams of the cerebral cortex in a glass/Teflon homogenizer tube (Iuchi) were homogenized in 2.2 ml 1% Triton X-100/MBS, pH 6.5, including a mixture of protease inhibitors (Complete; Boehringer Mannheim) with 10 up-and-down strokes at 3,000 rpm on ice. The homogenates were then sonicated at 4°C and incubated for 1 hr on ice. One hundred microliters of homogenate were then centrifuged at 100,000*g* for 1 hr at 4°C. The supernatant was removed and the resultant pellet was washed in MBS twice, resuspended in 50 μl of MBS, and subjected to highly sensitive immunoblot analysis with BA27 as a primary antibody.

Lipid Analysis

The concentrations of cholesterol and phospholipid in the samples were determined by using enzymatic methods as previously described (Gong et al., 2002). Cholesterol concentration was determined with a cholesterol determination kit, LTCII (Kyowa Medex, Tokyo, Japan), whereas phospholipid concentration was determined with a phospholipid determination kit, PLB (Wako, Osaka, Japan).

RESULTS AND DISCUSSION

Freshly dissolved Aβ1–40 remains as monomers, as demonstrated by immunoblot analysis and thioflavin-T assay as previously demonstrated (Zou et al., 2002). A rat brain was removed, and 100 mg of the cerebral cortex were isolated, to which 24 μl of 200 μM Aβ1– 40 were added. The cerebral cortex was then dissected into fragments in 2.2 ml of 1% Triton X-100/MBS containing protease inhibitors. The mixture was then homogenized with a glass/Teflon homogenizer (Iuchi) with 10 up-and-down strokes, followed by ultracentrifugation, as described in Materials and Methods. Samples from the 12 fractions were then obtained. The concentrations of cholesterol and phospholipids in each fraction were determined, and the recovery of GM1, a lipid raft marker, was demonstrated by electrophoresis, followed by labeling with horseradish peroxidase-conjugated choleatoxin. For the sample with Aβ1– 40, the main distributions peak of the cholesterol and phospholipids were found in the raft fractions, fractions 4–6, and most flotilin-1 and GM1, both of which are raft markers, was recovered in fractions 5 and 6 (Fig. 1a,c,e), whereas transferrin receptor, a nonraft maker, was recovered in fractions 10–12. This indicates that fractions 5 and 6 are the raft fractions. Similar results were obtained for the sample without exogenously added Aβ1– 40 (Fig. 1b,d,f).

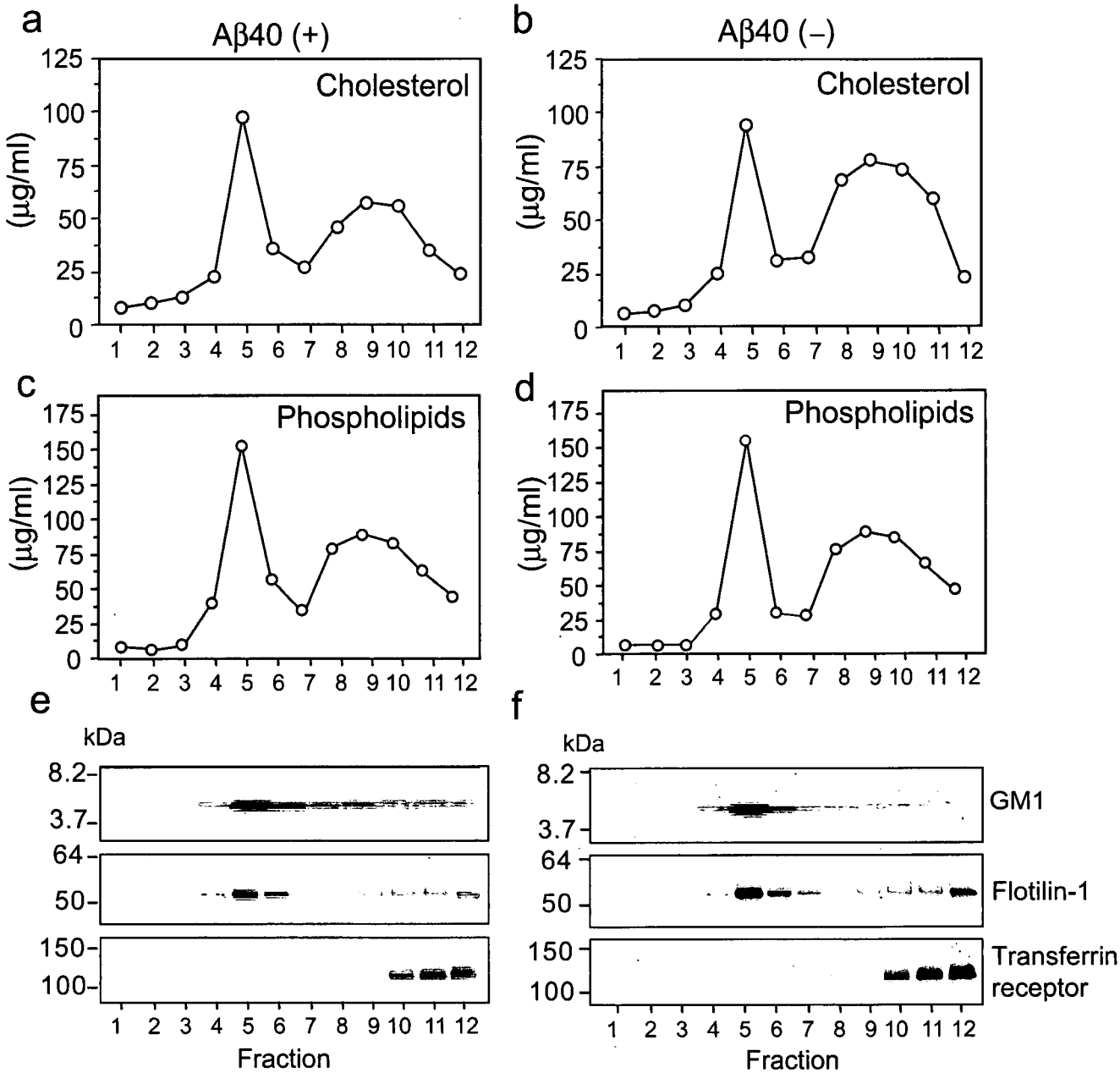

Fig. 1. Isolation of lipid raft fraction from a brain fragment with or without exogenous Aβ1– 40. The brain fragment was subjected to homogenization in the presence of 1% Triton X-100/MBS with Aβ1– 40 (2.1 μM; **a,c,e**) or without Aβ1–40 (**b,d,f**) and fractionated by sucrose density gradient centrifugation as described in Materials and Methods. The fractions were collected from the top gradient, and 11 fractions were obtained. The concentrations of cholesterol (**a,b**) and phospholipids (**c,d**) in each fraction were determined. The distribution of GM1 (**e,f**), a lipid raft marker, across the fractions was determined as described in Materials and Methods. Three independent experiments showed similar results.

We further analyzed the localization of Aβ1–40 in the above-mentioned fractions. Each sample was subjected to immunoblot analysis using the Aβ1–40-specific antibody BA27. Aβ1–40 accumulated and was highly oligomerized in fractions 4, 5, and 6 (Fig. 2a). No signal representing Aβ1–40 was detected in fraction 5, which was obtained by a method similar to that used for the sample without exogenously added Aβ1–40 (Fig. 2b). This indicates that signals representing the monomers and oligomers of Aβ1–40, as shown in Figure 2a, represent exogenously added Aβ1–40. We also analyzed a solution containing Aβ1–40 without a brain sample by sucrose-gradient ultracentrifugation, isolated fractions, and performed immunoblot analysis. Monomeric Aβ was detected in fractions 8–11, but no Aβ oligomers or Aβ accumulation were detected in the raft fraction (Fig. 2c). This is because the density of Aβ is higher

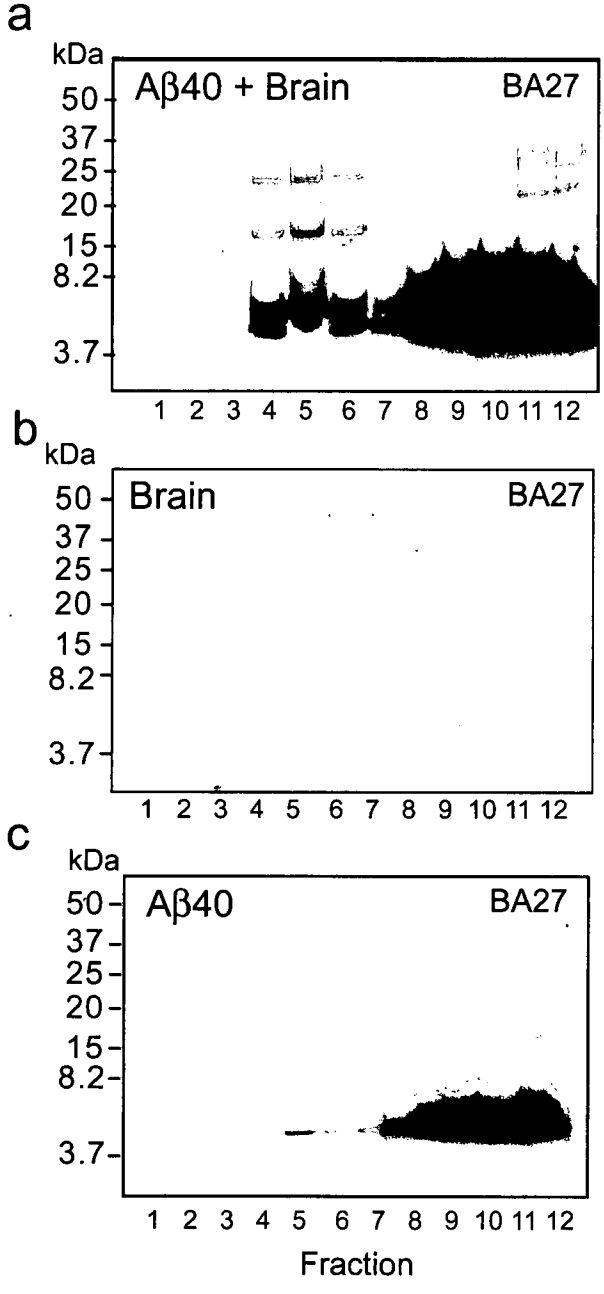

Fig. 2. Distribution of exogenously added Aβ1– 40 in lipid raft fractions. Brain fragments in the presence of 1% Triton X-100/MBS with (**a**) or without (**b**) exogenously added Aβ1– 40 (2.1 μM) were fractionated by sucrose density gradient centrifugation as described in Materials and Methods. Aβ1– 40 (2.1 μM) in 1% Triton X-100/MBS solution in the absence of brain fragments was also subjected to sucrose density gradient centrifugation (**c**). The fractions were collected from the top gradient, and 11 fractions were obtained. Immunoblot analysis using the anti-Aβ antibody BA27 was performed. Two independent experiments showed similar results.

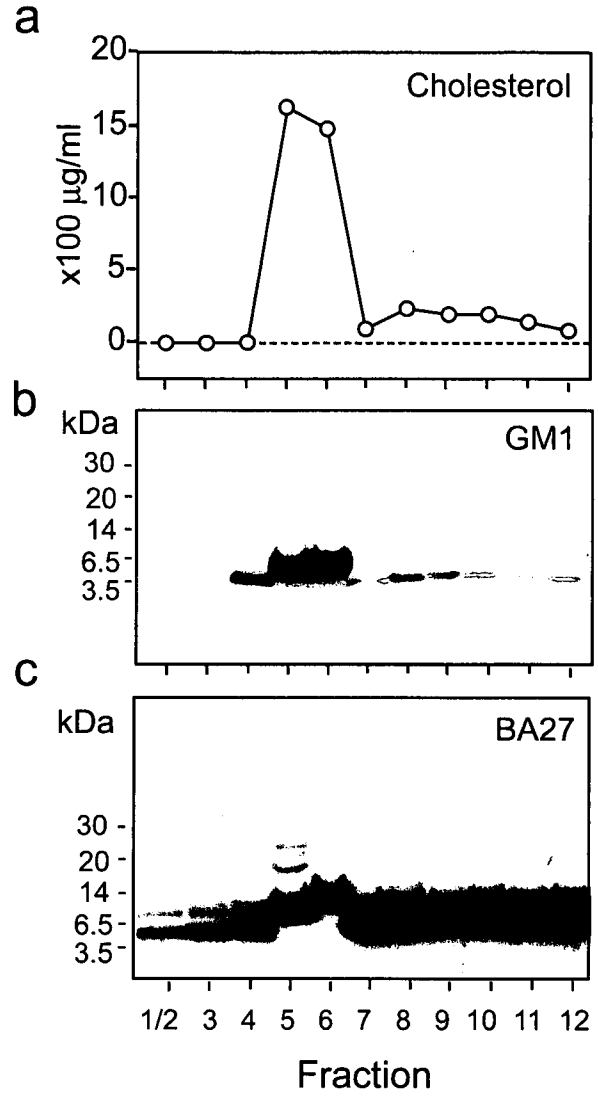

Fig. 3. Incubation of Aβ1– 40 in lipid rafts promoted Aβ1– 40 oligomerization. Brain homogenate in the presence of 1% Triton X-100/MBS without exogenously added Aβ1– 40 was fractionated by sucrose density gradient centrifugation as described in Materials and Methods. The distribution pattern of cholesterol (**a**) and GM1 (**b**) showed that fractions 5 and 6 are the lipid raft fractions. The aliquot of each fraction was incubated with 10 μM Aβ1– 40 for 20 hr at 4°C and subjected to immunoblot analysis using the anti-Aβ1–40 antibody BA27 (**c**).

than that of lipid rafts, so Aβ was recovered in fractions 8–11. The fact that exogenously added Aβ1–40 was recovered in the raft fraction indicates that Aβ1–40 binds to lipid rafts during the isolation of rafts, such as by homogenization, and that the binding of Aβ1–40 to lipid rafts leads to a shift in its localization to lower density fractions 4, 5, and 6.

Because the Aβ1–40 recovered in fraction 5 was highly oligomerized, we determined the effect of lipid rafts on Aβ oligomerization. We performed experiments to see the effect of incubating Aβ1–40 with raft and nonraft fractions on Aβ aggregation. The fractions were isolated from rat brain, and cholesterol concentration in each fraction was determined. The distribution patterns of cholesterol and GM1 across the fractions show that fractions 5 and 6 represent lipid raft fractions (Fig. 3a,b). The aliquot of each

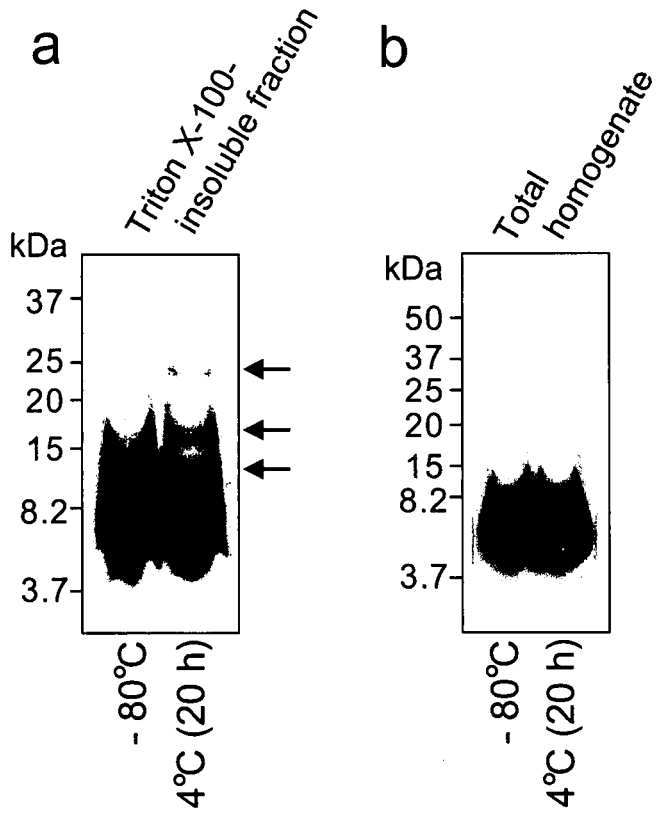

Fig. 4. Incubation of Triton X-100-insoluble fraction isolated from Tg2576 mouse brain promoted Aβ oligomerization. Brain homogenate from APP transgenic mouse (Tg2576) in the presence of 1% Triton X-100/MBS without exogenously added Aβ1–40 was centrifuged, and the Triton X-100-insoluble fraction was obtained as described in Materials and Methods. Aliquots of total homogenate and the Triton X-100-insoluble fraction were immediately frozen at –80°C until use. Aliquots of each sample were also incubated for 20 hr at 4°C. The protein concentration of these samples was adjusted to 1.5 mg/ml. An equal amount of protein of each sample (20 μg protein/lane) was used for immunoblot analysis using BA27. Results of immunoblot analysis of the Triton X-100-insoluble fraction and total homogenate are shown in **a** and **b**, respectively.

fraction was incubated with 10 μM Aβ1–40 for 20 hr at 4°C and was subjected to immunoblot analysis using the anti-Aβ1–40 antibody BA27. Immunoblot analysis showed a marked oligomerization of Aβ1–40 in raft fractions 5 and 6 (Fig. 3c). This indicates that lipid rafts have an ability to promote Aβ1–40 oligomerization compared with other fractions. This notion is supported by a series of works showing that raft-like membranes rich in cholesterol and GM1 promote Aβ aggregation (Kakio et al., 2001, 2002).

The present results show that the isolation of lipid rafts promotes Aβ1–40 oligomerization when Aβ1–40 is added exogenously. The question arises, however, of whether this is also the case for endogenous Aβ, because the concentration of exogenous Aβ used in this study was much higher than that of endogenous Aβ in the brain. Therefore, we examined whether endogenous Aβ forms aggregates during the isolation of lipid rafts from the brains of Tg2576 mice, which overexpress human APP695 with "Swedish" mutation. The oligomerization of endogenous Aβ was not detected in lipid raft fractions, probably because of the low level of Aβ generated even in Tg2576 mouse brains (data not shown). Interestingly, however, the oligomerization of endogenous Aβ occurred in the Triton X-100-insoluble fraction, when the fraction was incubated at 4°C for 20 hr (Fig. 4a, right lane, arrows), which is the same duration for the isolation of rafts, whereas it did not in a nonincubated sample (Fig. 4a, left lane). The oligomerization of endogenous Aβ was not detected in samples of total homogenate even after the incubation (Fig. 4b). These results suggest that endogenous Aβ might have a potential for forming oligomers during the isolation of lipid rafts from brains. Overall, one should be careful in drawing conclusions regarding the association of Aβ with lipid rafts in terms of Aβ localization, oligomerization, or degradation, if one uses mainly a biochemical method. Even if one uses other assays, such as morphological analysis, it is still possible to overestimate the extent of Aβ metabolism occurring in lipid rafts.

ACKNOWLEDGMENT

We thank Takeda Chemical Industries Ltd. for providing antibody BA27.

REFERENCES

Alzneimer A. 1907. Uber eine eigenartige Erkrankung der Hirnrinde. Centralbl Nervenheilk Pscychiatr 30:177–179.

Asami-Odaka A, Ishibashi Y, Kikuchi T, Kitada C, Suzuki N. 1995. Long amyloid beta-protein secreted from wild-type human neuroblastoma IMR-32 cells. Biochemistry 34:10272–10278.

Bagnat M, Keranen S, Shevchenko A, Simons K. 2000. Lipid rafts function in biosynthetic delivery of proteins to the cell surface in yeast. Proc Natl Acad Sci U S A 97:3254–3259.

Ehehalt R, Keller P, Haass C, Thiele C, Simons K. 2003. Amyloidogenic processing of the Alzheimer beta-amyloid precursor protein depends on lipid rafts. J Cell Biol 160:113–123.

Esiri M, Hyman B, Beyreuther K, Masters C. 1997. Aging and dementia, vol 2. London: Arnold. p 153–233.

Estus S, Tucker HM, van Rooyen C, Wright S, Brigham EF, Wogulis M, Rydel RE. 1997. Aggregated amyloid-beta protein induces cortical neuronal apoptosis and concomitant "apoptotic" pattern of gene induction. J Neurosci 17:7736–7745.

Fan QW, Yu W, Senda T, Yanagisawa K, Michikawa M. 2001. Cholesterol-dependent modulation of tau phosphorylation in cultured neurons. J Neurochem 76:391–400.

Geula C, Wu CK, Saroff D, Lorenzo A, Yuan M, Yankner BA. 1998. Aging renders the brain vulnerable to amyloid beta-protein neurotoxicity. Nat Med 4:827–831.

Gong JS, Kobayashi M, Hayashi H, Zou K, Sawamura N, Fujita SC, Yanagisawa K, Michikawa M. 2002. Apolipoprotein E (ApoE) isoform-dependent lipid release from astrocytes prepared from human ApoE3 and ApoE4 knock-in mice. J Biol Chem 277:29919–29926.

Gotz J, Chen F, van Dorpe J, Nitsch RM. 2001. Formation of neurofibrillary tangles in P301l tau transgenic mice induced by Abeta 42 fibrils. Science 293:1491–1495.

Harder T, Simons K. 1997. Caveolae, DIGs, and the dynamics of sphingolipid-cholesterol microdomains. Curr Opin Cell Biol 9:534–542.

Hartley DM, Walsh DM, Ye CP, Diehl T, Vasquez S, Vassilev PM, Teplow DB, Selkoe DJ. 1999. Protofibrillar intermediates of amyloid beta-protein induce acute electrophysiological changes and progressive neurotoxicity in cortical neurons. J Neurosci 19:8876–8884.

Hsiao K, Chapman P, Nilsen S, Eckman C, Harigaya Y, Younkin S, Yang F, Cole G. 1996. Correlative memory deficits, Abeta elevation, and amyloid plaques in transgenic mice. Science 274:99–102.

Kakio A, Nishimoto SI, Yanagisawa K, Kozutsumi Y, Matsuzaki K. 2001. Cholesterol-dependent formation of GM1 ganglioside-bound amyloid beta-protein, an endogenous seed for Alzheimer amyloid. J Biol Chem 276:24985–24990.

Kakio A, Nishimoto S, Yanagisawa K, Kozutsumi Y, Matsuzaki K. 2002. Interactions of amyloid beta-protein with various gangliosides in raft-like membranes: importance of GM1 ganglioside-bound form as an endogenous seed for Alzheimer amyloid. Biochemistry 41:7385–7390.

Kawarabayashi T, Shoji M, Younkin LH, Wen-Lang L, Dickson DW, Murakami T, Matsubara E, Abe K, Ashe KH, Younkin SG. 2004. Dimeric amyloid beta protein rapidly accumulates in lipid rafts followed by apolipoprotein E and phosphorylated tau accumulation in the Tg2576 mouse model of Alzheimer's disease. J Neurosci 24:3801–3809.

Kojro E, Gimpl G, Lammich S, Marz W, Fahrenholz F. 2001. Low cholesterol stimulates the nonamyloidogenic pathway by its effect on the alpha-secretase ADAM 10. Proc Natl Acad Sci U S A 98:5815–5820.

Koudinov AR, Koudinova NV. 2001. Essential role for cholesterol in synaptic plasticity and neuronal degeneration. FASEB J 15:1858–1860.

Lambert MP, Barlow AK, Chromy BA, Edwards C, Freed R, Liosatos M, Morgan TE, Rozovsky I, Trommer B, Viola KL, Wals P, Zhang C, Finch CE, Krafft GA, Klein WL. 1998. Diffusible, nonfibrillar ligands derived from Abeta1–42 are potent central nervous system neurotoxins. Proc Natl Acad Sci U S A 95:6448–6453.

Lee SJ, Liyanage U, Bickel PE, Xia W, Lansbury PT Jr, Kosik KS. 1998. A detergent-insoluble membrane compartment contains A beta in vivo. Nat Med 4:730–734.

Lisanti MP, Scherer PE, Vidugiriene J, Tang Z, Hermanowski-Vosatka A, Tu YH, Cook RF, Sargiacomo M. 1994. Characterization of caveolin-rich membrane domains isolated from an endothelial-rich source: implications for human disease. J Cell Biol 126:111–126.

Lorenzo A, Yankner BA. 1994. Beta-amyloid neurotoxicity requires fibril formation and is inhibited by Congo red. Proc Natl Acad Sci U S A 91:12243–12247.

Mattson MP, Tomaselli KJ, Rydel RE. 1993. Calcium-destabilizing and neurodegenerative effects of aggregated β-amyloid peptide are attenuated by basic FGF. Brain Res 621:35–49.

Michikawa M, Gong JS, Fan QW, Sawamura N, Yanagisawa K. 2001. A novel action of Alzheimer's amyloid β-protein (Aβ): oligomeric Aβ promotes lipid release. J Neurosci 21:7226–7235.

Morishima Y, Gotoh Y, Zieg J, Barrett T, Takano H, Flavell R, Davis RJ, Shirasaki Y, Greenberg ME. 2001. Beta-amyloid induces neuronal apoptosis via a mechanism that involves the c-Jun N-terminal kinase pathway and the induction of Fas ligand. J Neurosci 21:7551–7560.

Morishima-Kawashima M, Ihara Y. 1998. The presence of amyloid beta-protein in the detergent-insoluble membrane compartment of human neuroblastoma cells. Biochemistry 37:15247–15253.

Oshima N, Morishima-Kawashima M, Yamaguchi H, Yoshimura M, Sugihara S, Khan K, Games D, Schenk D, Ihara Y. 2001. Accumulation of amyloid beta-protein in the low-density membrane domain accurately reflects the extent of beta-amyloid deposition in the brain. Am J Pathol 158:2209–2218.

Pike CJ, Burdick D, Walencewicz AJ, Glabe CG, Cotman CW. 1993. Neurodegeneration induced by β-amyloid peptides in vitro: the role of peptide assembly state. J Neurosci 13:1676–1687.

Sargiacomo M, Sudol M, Tang Z, Lisanti MP. 1993. Signal transducing molecules and glycosyl-phosphatidylinositol-linked proteins form a caveolin-rich insoluble complex in MDCK cells. J Cell Biol 122:789–807.

Sawamura N, Gong JS, Garver WS, Heidenreich RA, Ninomiya H, Ohno K, Yanagisawa K, Michikawa M. 2001. Site-specific phosphorylation of tau accompanied by activation of mitogen-activated protein kinase (MAPK) in brains of Niemann-Pick type C mice. J Biol Chem 276:10314–10319.

Sawamura N, Ko M, Yu W, Zou K, Hanada K, Suzuki T, Gong JS, Yanagisawa K, Michikawa M. 2004. Modulation of amyloid precursor protein cleavage by cellular sphingolipids. J Biol Chem 279:11984–11991.

Selkoe DJ. 1994. Alzheimer's disease: a central role for amyloid. J Neuropathol Exp Neurol 53:438–447.

Simons K, Ikonen E. 1997. Functional rafts in cell membranes. Nature 387:569–572.

Simons M, Keller P, De Strooper B, Beyreuther K, Dotti CG, Simons K. 1998. Cholesterol depletion inhibits the generation of β-amyloid in hippocampal neurons. Proc Natl Acad Sci U S A 95:6460–6464.

Sponne I, Fifre A, Drouet B, Klein C, Koziel V, Pincon-Raymond M, Olivier JL, Chambaz J, Pillot T. 2003. Apoptotic neuronal cell death induced by the nonfibrillar amyloid-beta peptide proceeds through an early reactive oxygen species-dependent cytoskeleton perturbation. J Biol Chem 278:3437–3445.

Sudoh S, Kawamura Y, Sato S, Wang R, Saido TC, Oyama F, Sakaki Y, Komano H, Yanagisawa K. 1998. Presenilin 1 mutations linked to familial Alzheimer's disease increase the intracellular levels of amyloid beta-protein 1-42 and its N-terminally truncated variant(s) which are generated at distinct sites. J Neurochem 71:1535–1543.

Walsh DM, Klyubin I, Fadeeva JV, Cullen WK, Anwyl R, Wolfe MS, Rowan MJ, Selkoe DJ. 2002. Naturally secreted oligomers of amyloid beta protein potently inhibit hippocampal long-term potentiation in vivo. Nature 416:535–539.

Zou K, Gong JS, Yanagisawa K, Michikawa M. 2002. A novel function of monomeric amyloid beta-protein serving as an antioxidant molecule against metal-induced oxidative damage. J Neurosci 22:4833–4841.

Available online at www.sciencedirect.com

SCIENCE DIRECT

Brain Research 1043 (2005) 218–224

BRAIN RESEARCH

www.elsevier.com/locate/brainres

Short communication

Substance P immunoreactive cell reductions in cerebral cortex of Niemann–Pick disease type C mouse

Myeung Ju Kim[a], Jaewoo Kim[b], Brian Hutchinson[b], Makoto Michikawa[c], Choong Ik Cha[d], Bonghee Lee[b,e,*]

[a]*Department of Anatomy, Dankook University College of Medicine, Anseo-dong, Cheonan-si, Chungnam, South Korea*
[b]*Department of Anatomy, Cheju National University College of Medicine, 1 Ara 1 Dong, Jeju, Jeju-do 690-756, South Korea*
[c]*Section of Pathophysiology and Neurobiology, Department of Alzheimer's Disease Research, National Institute for Longevity Sciences, 36-3 Gengo, Morioka, Obu, Aichi 474-8522, Japan*
[d]*Department of Anatomy, Seoul National University College of Medicine, 28 Yongon-Dong, Chongno-Gu, Seoul 110-799, South Korea*
[e]*Institute of Medical Science, Cheju National University College of Medicine, Ara 1 Dong, Jeju, Jeju-do 690-756, South Korea*

Accepted 4 February 2005
Available online 1 April 2005

Abstract

Niemann–Pick disease type C (NPC) is characterized by progressive neurodegeneration and arises from mutations in the NPC1 gene. Cholesterol has received most attention in the pathogenesis of NPC, but normalizing lipid levels in humans or mouse does not prevent neurodegeneration. In NPC mouse, neuronal degeneration in the cerebellum is the most commonly detected change, and thus previous studies have tended to focus on the cerebellum, especially Purkinje cells. Although numerous peptides have been found in the mammalian central nervous system, little data on neurotransmitters in NPC are available, and information on neurotransmitter system abnormalities could explain the complex and characteristic deficits of NPC. Thus, we performed an immunohistochemical study on NPC mouse cortices to compare cell numbers exhibiting vasoactive intestinal polypeptide (VIP), neuropeptide Y (NPY), and substance P (SP) immunoreactivity. In terms of VIP and NPY-immunoreactive (ir) cell numbers in the cerebral cortex, SP-ir cells were significantly reduced by about 90% in NPC $^{(-/-)}$ versus NPC $^{(+/+)}$ mouse, and were also mildly decreased in frontal and parietal NPC $^{(+/-)}$ versus NPC $^{(+/+)}$ mouse cortex. This study demonstrates for the first time, reduced number of SP-ir cells in the NPC mouse cortex.
© 2005 Elsevier B.V. All rights reserved.

Theme: Disorders of the nervous system
Topic: Degenerative disease: other

Keywords: Niemann–Pick disease type C (NPC); Mouse cortex; Vasoactive intestinal polypeptide (VIP); Neuropeptide Y (NPY); Substance P (SP); Immunohistochemistry

Niemann–Pick disease type C (NPC) arises from mutations in the NPC1 gene on chromosome 18 [3], and is a fatal autosomal recessive neurovisceral disorder [21] characterized by the progressive neurodegeneration of the central nervous system (CNS) [6], which leads to premature death [23]. Cells lacking functional NPC1 accumulate cholesterol in the lysosomal and late endosomal compartments [12]. Cellular lesions in NPC patients are characterized by impaired LDL (low-density lipoprotein)-derived cholesterol transport from lysosomes, which results in lysosomal cholesterol sequestration [28]. In addition to cholesterol, neutral glycolipids and monosialogangliosides accumulate in the brains of NPC patients [23]. These lipid disturbances are essentially localized to gray matter. NPC patients exhibit increasing loss of motor control, seizures, and other neuropathological symptoms [22]. Like other lysosomal storage diseases, NPC disease is associated with

* Corresponding author. Department of Anatomy, Cheju National University College of Medicine, 1 Ara 1 Dong, Jeju, Jeju-do 690-756, South Korea. Fax: +82 64 702 2687.
E-mail address: bhlee1@cheju.ac.kr (B. Lee).

0006-8993/$ - see front matter © 2005 Elsevier B.V. All rights reserved.
doi:10.1016/j.brainres.2005.02.052

axonal abnormalities (spheroids, meganeurites, and axonal dystrophy) and demyelination of the corpus callosum [8]. A similar metabolic disorder has been previously described in Balb/C [27] and C57Bl/KsJ mouse [1]. Every organ manifests an accumulation of unesterified cholesterol and thus the whole body pool of sterol increases almost 3-fold by the time these animals are 11 weeks old [8]. Many neurons in the central nervous system show similar cholesterol-rich inclusions, as evidenced by positive fluorescence in filipin-stained brain sections [14]. However, normalizing lipid levels in humans and mouse does not prevent neurodegeneration [23]. Furthermore, evidence indicates that the concentrations of cholesterol and of its cytotoxic oxygenated derivatives are not increased in the brain of NPC mouse [24]. Therefore, a single mechanism associated with lipid or cholesterol is unlikely to account for NPC pathology.

Numerous peptides are found in the mammalian central nervous system. Neuropeptides found in high concentrations in the cerebral cortex include vasoactive intestinal polypeptide (VIP), neuropeptide Y (NPY), and substance P (SP) [4]. Thus, details of abnormalities of neurotransmitter and of their receptors could explain the complex and characteristic deficits of NPC [5], and comparisons between NPC neurotransmitter systems at disease onset and in the non-pathogenic state could be highly informative. However, previous studies on neurotransmitter expression in NPC mouse have focused primarily on the cerebellum, and especially on Purkinje cells, since neuronal degeneration in the cerebellum and associated brain stem structures is the most commonly detected change in NPC mouse, and is consistent with the development of tremor and ataxia [24]. However, a few have attempted to characterize the cell contents of regions like the cerebral cortex. Yadid et al. [28] found increased gamma amino butyric acid (GABA) and reduced serotonin levels in the NPC mouse cortex. These may be linked to the altered mouse exploratory behavior because GABA and serotonin are major regulators of emotional behavior like fear and anxiety [28]. Thus, we conjectured that changes in neurotransmitters or neuropeptides distributions in the cortex of NPC model mouse might provide information concerning NPC. We were particularly interested in the changes of immunoreactive (ir) cell number, which were stained by various neurotransmitters such as VIP, NPY, and SP. In this study, we quantitatively determined the cell numbers showing the VIP, NPY, and SP immunoreactivity (IR) using immunohistochemistry in the homogenously NPC 1 mutated mouse (−/−) cortex and compared these with those of the heterogenous (+/−) and wild (+/+) types.

BALB/c mice carrying the mutated NPC 1 gene were originally obtained from Dr. Michikawa (Dementia Research, NILS, Aichi, Japan) [15]. The mouse used in this study was 11 weeks old. For each VIP, NPY, and SP antibody, six NPC $^{(+/+)}$, five NPC $^{(+/-)}$, and five NPC $^{(-/-)}$ animals of both sexes were used. Additionally, we used all three types of mouse [six NPC $^{(+/+)}$, five NPC $^{(+/-)}$, and five NPC $^{(-/-)}$] at 4 weeks of age to compare developmental SP-ir cell number changes. Animals were treated in accordance with the *NIH Guide for the Care and Use of Laboratory Animals* (NIH publication No. 80-23, revised in 1996). Animals were anesthetized with pentobarbital (100 mg/kg, i.p.) and perfused transcardially with ice-cold 4% paraformaldehyde in 0.02 M phosphate-buffered saline (PBS, pH 7.4). Brains were cryoprotected in a series of cold sucrose solutions, and sectioned coronally at 30 μm on a cryostat. Immunohistochemistry was performed using the previously described free-floating method [4]. Rabbit anti-rat VIP (Diasorin, Cat No. 20077), NPY (Diasorin, Cat. No. 22940), and SP (Diasorin, Cat. No. 20064) antibodies were used as main primary antibodies at a final concentration of 1.5 mg/ml. In addition, we used another SP primary antibody (Chemicon, Cat No. MAB 356 at a dilution ratio of 1:3000) to certify the reliability of our immunohistochemical staining results. Some of the sections were reacted without primary antiserum, whereas others were exposed to a primary antiserum (0.06 mg/ml) that had been preabsorbed for 24 h with cognate peptide (0.1 mg/ml). No NPC $^{(+/+)}$ mouse brain sections showed any of the IR described in this report (Figs. 1B, C). All three types of mouse brain sections were stained together, thus eliminating experimental condition differences. To determine whether cell loss had occurred in NPC $^{(-/-)}$ mouse, we performed cresyl-violet staining in the mouse cortex. However, in 11-week-old NPC $^{(-/-)}$ mouse, we did not find any significant decrease in cell numbers in all the cortices of NPC $^{(-/-)}$ versus NPC $^{(+/+)}$ or NPC $^{(+/-)}$ by cresyl-violet staining (Figs. 1C–E). For the comparative analysis of neurotransmitters (VIP, NPY, SP), we selected 5 slides of each cortical area from each mouse, and counted all specifically stained cells in corresponding areas (Tables 1, 2) of mouse cerebral cortex for each primary antibody by optical microscopy. The Student's *t* test was used to determine whether changes in ir cell numbers in each cortical area were statistically significant (Table 2).

Prominent VIP-ir cells were observed throughout the cortices of three mouse types [NPC $^{(+/+)}$, NPC $^{(+/-)}$, NPC $^{(-/-)}$]. These were mainly present in layers II and III (Figs. 2A–C) although they were distributed in all layers of the cerebral cortex. VIP-ir cells were predominantly bipolar, i.e., with ovoid somata and dendrites oriented perpendicular to the pial surface (Figs. 2A–C). This distribution pattern was well preserved and no significant differences were observed between the cortices of the three mouse types (Figs. 2A–C, Table 1). NPY-IR showed a preferential distribution in cells of the II/III and V/VI layers. Cortical cells exhibited NPY-IR in the dendritic trees of bipolar and multipolar arrangements, and their cell bodies were fully stained in all three mouse types (Figs. 2G–I). When we compared all three mouse types, we were unable to find notable differences in the number of NPY-ir cells across mouse cortical areas (Table 2). A slight decrease of NPY-ir cell number was observed in the retrosplenial granular/

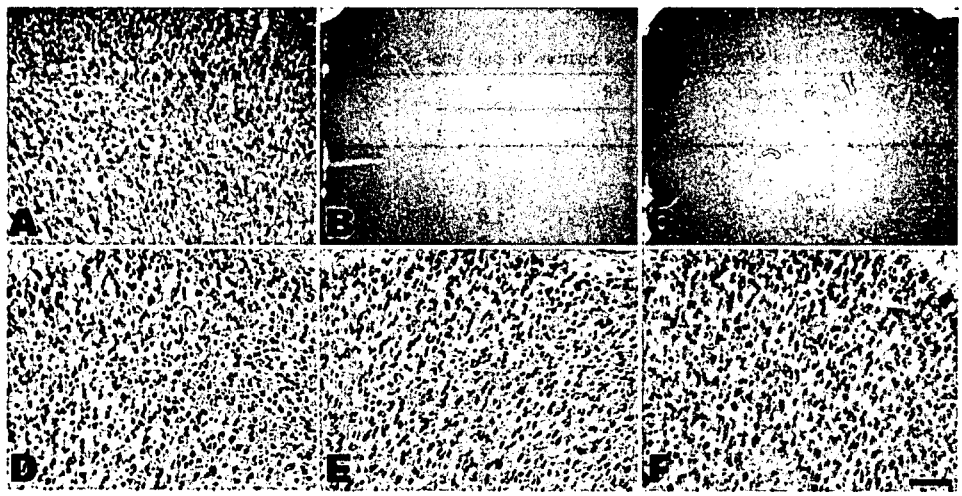

Fig. 1. In the frontal cortex area 1 of 11-week-old NPC $^{(+/+)}$ mouse, the SP (Chemicon, Cat No. MAB 356) immunoreactivities (IR) were largely confined to cell bodies and their proximal dendrites of IV–VI layers (A). By cresyl-violet staining, there were no cell number differences in the 11-week-old NPC $^{(-/-)}$ mouse (F) versus age-matched NPC $^{(+/+)}$ (D) or NPC $^{(+/-)}$ (E) mouse cortex. Sections that were reacted with primary SP antiserum [Cat. No. 20064 (B), and MAB 356 (C)] that had been preincubated for 24 h with cognate peptide did not exhibit any IR. Scale bars = 100 μm in A, D, E, F, 200 μm in B, C.

agranular NPC $^{(-/-)}$ compared with NPC $^{(+/+)}$ cortex (Table 1), where some individual variations in the NPY-ir cell number were present. In the 11-week-old NPC $^{(+/+)}$ mouse cortex, many SP-ir cell bodies were observed in the frontal, parietal, temporal, and occipital cortex. SP-ir cell bodies were observed in layers II–VI, and the majority of cells in NPC $^{(+/+)}$ mouse were bipolar or multipolar in shape (Fig. 2D). In the deeper layers of the 11-week-old NPC $^{(+/+)}$ mouse cortex, particularly layers V and VI, many arrays of SP-containing fibers were observed (Fig. 2D). These fibers were oriented perpendicular to the pial surface, and appeared to be fibers of passage with few varicosities (Figs. 2D, 3J). SP-ir cells in 11-week-old NPC $^{(+/-)}$ mouse (Figs. 2E, 3B, E, H) were similar in pattern to those in NPC $^{(+/+)}$ mouse (Figs. 2D, 3A, D, G) and were observed across all cortical areas. The number of SP-ir cells was severely decreased (>70%) in all areas of the 11-week-old NPC $^{(-/-)}$ mouse cortex (Figs. 2F, 3C, F, I, K) versus those of NPC $^{(+/+)}$ mouse (Figs. 2D, 3A, D, G, J, Tables 1, 2). When compared with 11-week-old NPC $^{(+/+)}$ mouse, changes in 11-week-old NPC $^{(+/-)}$ were variable in each cortical area. Moderate (50–70%) SP-ir cell reductions were observed in the frontal cortex 1 (Fig. 2E, Tables 1, 2), 2, and 3 and parietal cortex 1 (Figs. 3A–C, Tables 1, 2). Mild (15–50%) SP-ir cell reductions were observed in the parietal

Table 1
The number of VIP, NPY, and SP-ir neurons in each area of NPC $^{(+/+)}$, NPC $^{(+/-)}$, and NPC $^{(-/-)}$ mice cerebral cortex

		VIP			NPY			SP		
		(+/+)	(+/−)	(−/−)	(+/+)	(+/−)	(−/−)	(+/+)	(+/−)	(−/−)
Frontal	Fr1	78.1 ± 5.7	77.5 ± 4.3	76 ± 5.5	35.5 ± 5.7	35.7 ± 6.2	36.1 ± 4.9	673.2 ± 56.9	315.9 ± 36.9	34.2 ± 5.3
	Fr2	35.1 ± 8.9	35.2 ± 9.3	34.9 ± 10.2	23.8 ± 2.4	24.6 ± 8.1	23.3 ± 1.4	302.6 ± 37.3	143.1 ± 32.0	25.6 ± 2.6
	Fr3	51.6 ± 5.2	49.9 ± 9.8	52.1 ± 9.7	37.8 ± 8.4	38.1 ± 2.1	36.9 ± 10.6	441.3 ± 18.7	202.8 ± 10.6	13.3 ± 1.9
Cingulate		53.2 ± 6.4	53.8 ± 7.7	52.5 ± 7.4	32.6 ± 1.0	32.1 ± 6.3	30.4 ± 4.3	438.4 ± 24.9	415.5 ± 22.8	12.9 ± 2.6
Parietal	Par1	79.3 ± 2.4	80.1 ± 5.3	79.4 ± 8.6	21.7 ± 6.8	20.8 ± 1.4	21.9 ± 7.1	620.1 ± 53.4	390.8 ± 31.5	68.3 ± 7.4
	Par2	67.5 ± 5.1	68.3 ± 9.2	66 ± 6.9	19.1 ± 5.2	18.8 ± 2.7	18.6 ± 6.7	525.8 ± 64.8	432.5 ± 27.3	56.5 ± 2.8
Temporal	Te1	72.8 ± 3.5	71.6 ± 10.8	72.3 ± 7.2	23.7 ± 8.3	22.5 ± 9.4	23.1 ± 1.5	403.4 ± 46.1	389 ± 21.3	92.7 ± 7.1
	Te2	77.4 ± 5.5	77.1 ± 4.6	76.9 ± 8.3	18.0 ± 4.8	19.5 ± 4.2	17.6 ± 2.4	433.2 ± 29.8	428.6 ± 33.2	97.9 ± 10.7
	Te3	52.8 ± 8.2	52.6 ± 5.4	53 ± 5.7	17.1 ± 8.2	18.8 ± 2.1	17.3 ± 7.4	295.5 ± 18.7	292.4 ± 16.2	67.4 ± 9.3
Occipital	Oc2M	73.8 ± 6.2	73.6 ± 10.4	74 ± 8.7	33.8 ± 8.9	36.8 ± 7.9	36.5 ± 5.9	632.8 ± 21.7	598.1 ± 23.9	43.9 ± 5.2
	Oc2L	56.2 ± 6.2	55.8 ± 5.5	56.1 ± 9.5	23.6 ± 3.6	24.8 ± 3.5	24.3 ± 6.2	481.3 ± 42.3	468.5 ± 35.6	32.6 ± 2.4
	Oc1M	49.5 ± 9	48.9 ± 5	48.5 ± 8.2	25.3 ± 6.4	24.7 ± 2.8	25.1 ± 4.3	423.9 ± 29.6	409.6 ± 32.5	28.2 ± 1.3
	Oc1B	81.2 ± 6.2	80.2 ± 4.3	80.6 ± 5.4	28.8 ± 8.7	27.9 ± 1.8	28.2 ± 3.2	685.4 ± 63.1	653.4 ± 70.8	46.8 ± 3.4
Perirhinal area		76.1 ± 8.2	76.8 ± 9.1	76.5 ± 8.3	17.9 ± 9.1	17.5 ± 7.4	16.9 ± 8.4	68.2 ± 15.7	59.2 ± 13.6	8.8 ± 2.2
Retrosplenial granular and agranular cortex		52 ± 4.8	51.7 ± 8.6	51.8 ± 8.9	21.7 ± 2.2	17.6 ± 4.5	18.5 ± 3.9	467.8 ± 38.4	413.5 ± 52.3	13.4 ± 1.7
Piriform cortex		67.5 ± 11.3	66.8 ± 8.3	67 ± 9.6	13.0 ± 3.8	12.4 ± 2.9	13.1 ± 4.5	187.0 ± 25.3	172.2 ± 21.9	10.3 ± 2.5

Data = means ± SE. (+/+) = NPC $^{(+/+)}$; (+/−) = NPC $^{(+/-)}$; (−/−) = NPC $^{(-/-)}$.

Table 2
Changes of the numbers of VIP, NPY, and SP-immunoreactive neurons in each area of the NPC $^{(+/-)}$, NPC $^{(-/-)}$[a]

Area	Subdivision	VIP		NPY		SP	
		(+/−)	(−/−)	(+/−)	(−/−)	(+/−)	(−/−)
Frontal	Fr1	0	0	0	0	−−[b]	−−−[b]
	Fr2	0	0	0	0	−−[b]	−−−[b]
	Fr3	0	0	0	0	−−[b]	−−−[b]
Cingulate		0	0	0	0	0	−−−[b]
Parietal	Par1	0	0	0	0	−−[b]	−−−[b]
	Par2	0	0	0	0	−[b]	−−−[b]
Temporal	Te1	0	0	0	0	0	−−−[b]
	Te2	0	0	0	0	0	−−−[b]
	Te3	0	0	0	0	0	−−−[b]
Occipital	Oc2M	0	0	0	0	0	−−−[b]
	Oc2L	0	0	0	0	0	−−−[b]
	Oc1M	0	0	0	0	0	−−−[b]
	Oc1B	0	0	0	0	0	−−−[b]
Perirhinal area		0	0	0	0	0	−−−[b]
Retrosplenial granular and agranular cortex		0	0	−	0	0	−−−[b]
Piriform cortex		0	0	0	0	0	−−−[b]

[a] The data were classified into 4 categories comparing the immunoreactive (ir) cell number in NPC (+/−), NPC (−/−) with ir cell number of NPC (+/+) according to the % of counted cell number [0, no change (−15–15%); −, mild decrease (15–50%);− −, moderate decrease (50–75%);− − −, severe decrease (>75%)] and counted the number of cells graded '0, −, − −, − − −'.
[b] Statistically significant area ($P < 0.05$).

cortex 2 (Tables 1, 2). In particular, few cells showed SP-IR in the occipital cortex (Fig. 3I). At the cellular level, SP-IR in the 11-week-old NPC $^{(+/+)}$ mouse cortex was mainly localized in cell bodies and cytoplasmic processes (Fig. 3J). However, dendrites of SP-ir cells in the cortex of 11-week-old NPC $^{(-/-)}$ mouse were markedly shorter and barely observed (Fig. 3K). Morphologically, the dendrites of SP-ir cells branched several times in 11-week-old NPC $^{(+/+)}$ mouse

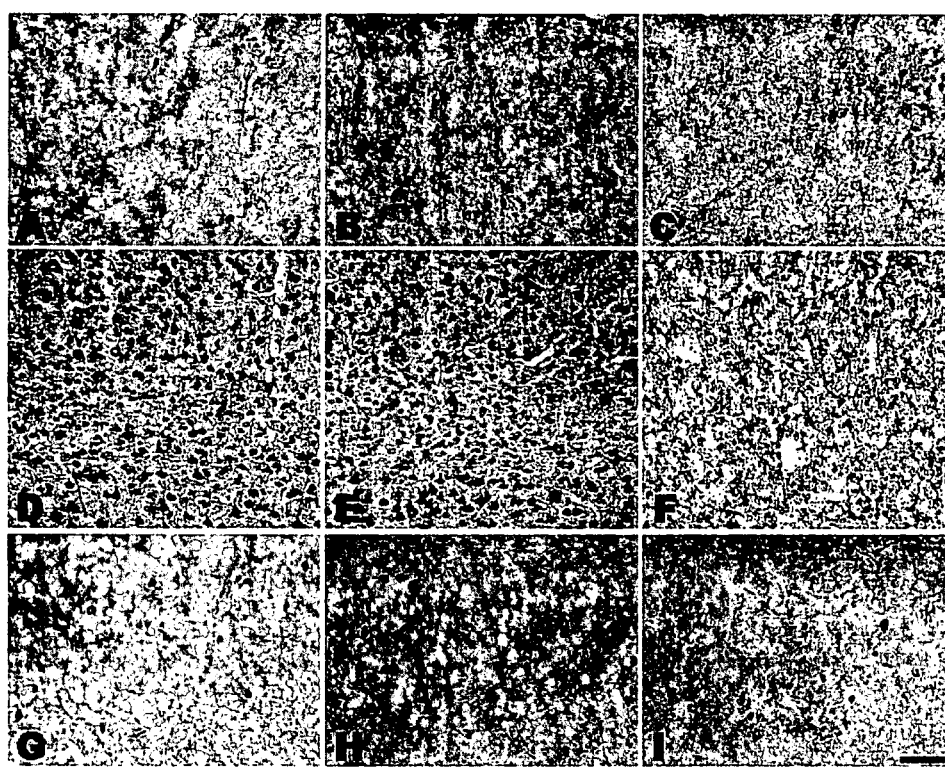

Fig. 2. Changes in the number of VIP (A, B, C), SP (D, E, F), and NPY (G, H, I) immunoreactive (ir) cells in the frontal cortex area 1 of NPC $^{(-/-)}$ (C, F, I), NPC $^{(+/-)}$ (B, E, H), and NPC $^{(+/+)}$ (A, D, G). A significant reduction of SP-ir cell number and the small number of shortened dendritic branches were observed in frontal cortex area 1 of the NPC $^{(-/-)}$ (F). VIP and NPY-ir cells in the frontal cortex area 1 show no significant differences among the three mice models. Scale bar = 100 μm.